板坂聡、 原田浩、 近藤科江、 平岡真寛	新しい分子イメージングの活用　1.新しい治療法評価への分子イメージングの応用　2.放射線治療の分子イメージング	遺伝子医学MOOK	9	279-283	2007

Available online at www.sciencedirect.com
ScienceDirect
Nuclear Medicine and Biology 34 (2007) 503–510
NUCLEAR MEDICINE — AND — BIOLOGY
www.elsevier.com/locate/nucmedbio

Chemical design of a radiolabeled gelatinase inhibitor peptide for the imaging of gelatinase activity in tumors

Hirofumi Hanaoka[a,b], Takahiro Mukai[c,d], Sayo Habashita[a], Daigo Asano[a], Kazuma Ogawa[a], Yoshihiro Kuroda[a], Hiromichi Akizawa[e], Yasuhiko Iida[b], Keigo Endo[b], Tsuneo Saga[c], Hideo Saji[a,*]

[a]*Graduate School of Pharmaceutical Sciences, Kyoto University, Yoshida Shimoadachi-cho, Kyoto 606-8501, Japan*
[b]*Graduate School of Medicine, Gunma University, Maebashi 371-8511, Japan*
[c]*Graduate School of Medicine, Kyoto University, Kyoto 606-8507, Japan*
[d]*Graduate School of Pharmaceutical Sciences, Kyushu University, Fukuoka 812-8582, Japan*
[e]*Graduate School of Pharmaceutical Sciences, Chiba University, Chiba 260-8675, Japan*

Received 27 March 2007; accepted 4 April 2007

Abstract

Since elevated levels of gelatinases [matrix metalloproteinase (MMP)-2 and MMP-9] are associated with a poor prognosis in cancer patients, these enzymes are potential targets for tumor imaging. In the present study, a cyclic decapeptide, cCTTHWGFTLC (CTT), was selected as a mother compound because of its selective inhibitory activity toward gelatinases. For imaging gelatinase activity in tumors, we designed a CTT-based radiopharmaceutical taking into consideration that (1) the HWGF motif of the peptide is important for the activity, (2) hydrophilic radiolabeled peptides show low-level accumulation in the liver and (3) an increase in the negative charge of radiolabeled peptides is effective in reducing renal accumulation. Thus, a highly hydrophilic and negatively charged radiolabel, indiun-111-diethylenetriamine-pentaacetic acid (^{111}In-DTPA), was attached to an N-terminal residue distant from the HWGF motif (^{111}In-DTPA-CTT). In MMP-2 inhibition assays, In-DTPA-CTT significantly inhibited the proteolytic activity in a concentration-dependent fashion. When injected into normal mice, ^{111}In-DTPA-CTT showed low levels of radioactivity in the liver and kidney. A comparison of the pharmacokinetic characteristics of ^{111}In-DTPA-CTT with those of other CTT derivatives having different physicochemical properties revealed that the increase in hydrophilicity and negative charge caused by the conjugation of ^{111}In-DTPA reduced levels of radioactivity in the liver and kidney. In tumor-bearing mice, a significant correlation was observed between the accumulation in the tumor as well as tumor-to-blood ratio of ^{111}In-DTPA-CTT and gelatinase activity. These findings support the validity of the chemical design of ^{111}In-DTPA-CTT for reducing accumulation in nontarget tissues and maintaining the inhibitory activity of the mother compound. Furthermore, ^{111}In-DTPA-CTT derivatives would be potential radiopharmaceuticals for the imaging of gelatinase activity in metastatic tumors in vivo.

Keywords: Gelatinase; Radiolabeled peptide; Liver; Kidney; Hydrophilicity; Electric charge

1. Introduction

Matrix metalloproteinases (MMPs) comprise a family of enzymes that degrade the basement membrane and extracellular matrix, thus contributing to tissue remodeling and cell migration [1,2]. The family includes several subgroups, one of which comprises the gelatinases MMP-2 (gelatinase A, 72-kD type IV collagenase) and MMP-9 (gelatinase B, 92-kD type IV collagenase). The expression of gelatinases in normal cells, such as trophoblasts, osteoclasts, neutrophils and macrophages, is tightly regulated, while many types of malignant tumors express higher levels of gelatinases than normal, possibly enabling tumor cells to invade the extracellular matrix and generate metastases at sites distant from the primary tumor [3–5]. Indeed, an enhanced or unregulated expression of MMP-2 and MMP-9 is associated with a poor prognosis in cancer patients [6–9]. Therefore, gelatinases are potential targets for tumor imaging.

* Corresponding author. Tel.: +81 75 753 4556; fax: +81 75 753 4568.
E-mail address: hsaji@pharm.kyoto-u.ac.jp (H. Saji).

0969-8051/$ – see front matter © 2007 Elsevier Inc. All rights reserved.
doi:10.1016/j.nucmedbio.2007.04.002

A large number of MMP inhibitors have been developed as therapeutic agents, some of which are currently in clinical trials [10–12]. The aim of this study was to develop a radiolabeled MMP inhibitor as a diagnostic agent for metastatic tumors. Among MMP inhibitors, we selected a cyclic decapeptide, cCTTHWGFTLC (CTT) [13], as the mother compound because of the clinical and radiopharmaceutical utility of peptide-based radiopharmaceuticals [14]. Considering that (1) the HWGF motif and cyclic disulfide-bonded structure of this hydrophobic peptide are important for its inhibitory activity [13], (2) increasing the hydrophilicity of radiolabeled peptides improves their excretion from a hepatobiliary to a urinary pathway [15,16] and (3) an increase in the negative charge of peptide molecules would be effective in lowering the renal accumulation of radiolabeled hydrophilic peptides [17,18], we attached a highly hydrophilic and negatively charged indiun-111-diethylenetriaminepentaacetic acid (^{111}In-DTPA) to an amino group of the N-terminal cysteine of the CTT peptide. In this study, the inhibitory effect of In-DTPA-CTT on the proteolytic activity of MMP-2 was compared with that of CTT. Furthermore, the hepatic and renal accumulations of radioactivity after administration of ^{111}In-DTPA-CTT were compared with those of radiolabeled CTT derivatives having different physicochemical properties. The structures of the radiolabeled CTT derivatives used in this study are shown in Fig. 1. Finally, the accumulation of ^{111}In-DTPA-CTT in tumors was compared with the gelatinase activity in tumor-bearing mice. From these comparisons, the validity of the chemical design of this peptide radiopharmaceutical for imaging gelatinase activity was assessed.

2. Materials and methods

2.1. General

Nonradioactive indium chloride was obtained from Nacalai Tesque (Kyoto, Japan) as $InCl_3 \cdot 4H_2O$. $^{111}InCl_3$ (74 MBq/ml in 0.02 N of HCl) was kindly supplied by Nihon Medi-Physics (Nishinomiya, Japan). Na^{125}I (3.7 GBq/ml in 5–10 N of NaOH) was purchased from PerkinElmer Life Sci (Boston, MA, USA). Fmoc-Thr(^{t}Bu), Fmoc-Trp(Boc), Fmoc-Gly, Fmoc-Phe and Fmoc-Leu (where Fmoc, ^{t}Bu and Boc are 9-fluorenylmethoxycarbonyl, *tert*-butyl and *tert*-butyloxycarbonyl, respectively) were obtained from Novabiochem (Läufelfingen, Switzerland). Cys(Acm)-loaded 2-chlorotrityl chloride resin, Fmoc-Cys(Acm), Fmoc-His(Trt), Fmoc-D-Asn(Trt) and Fmoc-D-Lys(Boc) (where Acm and Trt are acetamidomethyl and trityl, respectively) were purchased from Watanabe Chemical Industries (Hiroshima, Japan). 1-*tert*-Butyl hydrogen 3,6,9-tris(*tert*-butoxycarbonyl)methyl-3,6,9-triazaundecanedioic acid (mDTPA) was synthesized as reported [19]. *N*-Succinimidyl-3-[^{125}I]iodobenzoate ([^{125}I]SIB) was prepared according to procedures described previously [20]. MDA-MB-231 and MDA-MB-435S (human breast cancer cell lines) were purchased from the American Type Culture Collection (Manassas, VA, USA). Ion-spray mass spectra (IS-MS) and electrospray-ionization mass spectra (ESI-MS) were obtained with an API III model (PerkinElmer Sciex Instruments, Thornhill, Canada) and an LCMS-QP8000α model (Shimadzu, Kyoto, Japan), respectively. Other reagents were of reagent grade and used as received.

2.2. Peptide synthesis

The protected peptidyl resins were constructed automatically using an Fmoc-based solid-phase methodology on 2-chlorotrityl chloride resins with a peptide synthesizer (ABI 433A, Applied Biosystems, Foster City, CA, USA). mDTPA was conjugated to the N-terminus of each peptidyl resin as described previously [21]. Triethylsilane (125 μl), trifluoroacetic acid (TFA; 4.75 ml) and water (125 μl) were added to the peptidyl resins (100 mg), and the mixture was stirred at room temperature for 2 h. After the resins were removed by filtration, dry ether was added to precipitate crude peptides. The S-protected peptides were purified by high-performance liquid chromatography (HPLC; Cosmosil 5C_{18}-AR-300 column, 20×250 mm, Nacalai Tesque) eluted with a linear gradient of 20–30% acetonitrile in 0.1% aqueous TFA for 30 min at a flow rate of 15 ml/min. Fractions containing the peptides were collected, and the solvent was removed by lyophilization.

H-Cys(Acm)-Thr-Thr-His-Trp-Gly-Phe-Thr-Leu-Cys(Acm)-OH: ESI-MS calculated for $C_{58}H_{84}N_{15}O_{16}S_2$ ($M+H^+$); *m/z*, 1310.57; found, 1310.

DTPA-Cys(Acm)-Thr-Thr-His-Trp-Gly-Phe-Thr-Leu-Cys(Acm)-OH: ESI-MS calculated for $C_{72}H_{105}N_{18}O_{25}S_2$ ($M+H^+$); *m/z*, 1685.69; found, 1685.

DTPA-D-Asn-Cys(Acm)-Thr-Thr-His-Trp-Gly-Phe-Thr-Leu-Cys(Acm)-OH: ESI-MS calculated for $C_{76}H_{111}N_{20}O_{27}S_2$ ($M+H^+$); *m/z*, 1799.74; found, 1799.

DTPA-D-Lys-Cys(Acm)-Thr-Thr-His-Trp-Gly-Phe-Thr-Leu-Cys(Acm)-OH: ESI-MS calculated for $C_{78}H_{117}N_{20}O_{26}S_2$ ($M+H^+$); *m/z*, 1813.79; found, 1814.

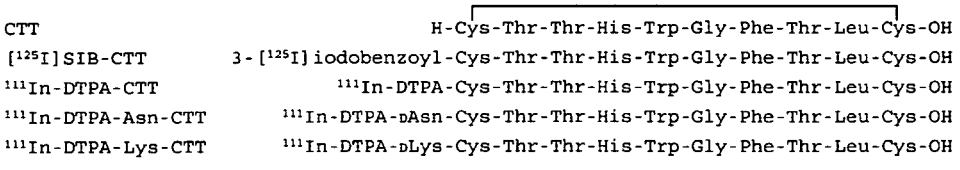

Fig. 1. Structures of radiolabeled CTT derivatives. The solid line depicts a disulfide linkage.

The S-protected peptides (10 mg) were dissolved in 80% acetic acid (10 ml). To this solution were added 1 N of HCl (1 ml) and 20% iodine in acetic acid (1 ml), and the mixture was stirred at room temperature for 1 h. The excess iodine was reduced with 1 M of aqueous ascorbic acid. Subsequent purification with HPLC was performed using the same column as cited, eluted with a linear gradient of 20–35% acetonitrile in 0.1% aqueous TFA for 45 min at a flow rate of 15 ml/min. Fractions containing the desired products were collected and lyophilized.

CTT: ESI-MS calculated for $C_{52}H_{72}N_{13}O_{14}S_2$ ($M+H^+$); *m/z*, 1166.48; found, 1166.

DTPA-CTT: IS-MS calculated for $C_{66}H_{93}N_{16}O_{23}S_2$ ($M+H^+$); *m/z*, 1541.60; found, 1542.5.

DTPA-Asn-CTT: ESI-MS calculated for $C_{70}H_{99}N_{18}O_{25}S_2$ ($M+H^+$); *m/z*, 1655.65; found, 1655.

DTPA-Lys-CTT: ESI-MS calculated for $C_{72}H_{105}N_{18}O_{24}S_2$ ($M+H^+$); *m/z*, 1669.70; found, 1669.

2.3. Radiolabeling

To each DTPA-conjugated peptide (10 μg, 50 μg/ml) in 0.1 M of acetic acid was added $^{111}InCl_3$ (3.7–7.4 MBq, 200 μl), and the mixture was incubated at room temperature for 30 min. Then, each ^{111}In-labeled peptide was purified by HPLC to exclude non-peptide-bound ^{111}In species and unchelated peptides. The purification was performed with a Hydrosphere C18 column (4.6×250 mm, YMC, Kyoto, Japan) eluted with a mixture of acetonitrile and 0.1% aqueous TFA (26:74 for ^{111}In-DTPA-CTT and ^{111}In-DTPA-Asn-CTT, 24:76 for ^{111}In-DTPA-Lys-CTT) at a flow rate of 1 ml/min. An appropriate amount of ethanol was added to fractions containing each ^{111}In-labeled peptide, and the solvent was removed in vacuo. Phosphate-buffered saline (20 mM, pH 7.4) containing 0.1% human serum albumin was added to the residue for biodistribution experiments. Radiochemical purities of ^{111}In-labeled peptides were determined by HPLC and thin-layer chromatography (TLC). The analytical HPLC column (Hydrosphere C18, 4.6×250 mm) was eluted with a mixture of acetonitrile and 0.1% aqueous TFA (27:73 for ^{111}In-DTPA-CTT and ^{111}In-DTPA-Asn-CTT, 26:74 for ^{111}In-DTPA-Lys-CTT) at a flow rate of 1 ml/min. The TLC plate (Silica gel 60, Merck, Darmstadt, Germany) was developed with 10% ammonium chloride/methanol (1:1).

Nonradioactive indium was reacted with DTPA-CTT to investigate the effect of the conjugation with ^{111}In-DTPA on the inhibition of the gelatinase by CTT as follows: a 1.1 molar excess of $InCl_3 \cdot 4H_2O$ in 0.02 N of HCl was added to DTPA-CTT in a mixture of 0.1 M of acetic acid and dimethylformamide (DMF; 1:1). After stirring at room temperature for 30 min, In-DTPA-CTT was purified by HPLC under the same conditions as for the purification of ^{111}In-DTPA-CTT. Fractions containing the desired products were collected and lyophilized. IS-MS calculated for In $C_{66}H_{90}N_{16}O_{23}S_2$ ($M+H^+$): *m/z*, 1653.58; found, 1653.5.

The radioiodination of CTT was achieved by conjugation with [^{125}I]SIB. Briefly, 50 μl of CTT (4 mg/ml) and 1-hydroxybenzotriazole monohydrate (2.6 mg/ml) in DMF was added to a reaction vial containing crude [^{125}I]SIB (7.4 MBq). To this solution was added 2 μl of 10% triethylamine–DMF, and the mixture was stirred at room temperature for 7 h. [^{125}I]SIB-CTT was purified by HPLC (Capcell Pak C18 ACR, 4.6×250 mm, Shiseido, Tokyo, Japan) eluted with a linear gradient of 30–40% acetonitrile in 0.1% aqueous TFA for 50 min at a flow rate of 1 ml/min.

2.4. MMP-2 inhibition assay

A 96-well microplate containing 2 nM of activated human recombinant MMP-2 (Oncogene Research Products, San Diego, CA, USA) and 0.5–1000 μM of In-DTPA-CTT or CTT in 50 mM of MOPS buffer (pH 7.0; 10 mM of $CaCl_2$, 10 μM of $ZnCl_2$, 0.05% Brij-35 and 5% dimethylsulfoxide) was placed in a fluid-handling integrated fluorometer (FlexStation, Molecular Devices, Sunnyvale, CA, USA) set to read fluorescence at 328 nm of excitation and 393 nm of emission. After incubation at 37°C for 30 min, a 10-μl aliquot of quenched fluorescent substrate solution (1 μM of the final concentration, OmniMMP, Biomol Research Laboratories, Plymouth Meeting, PA, USA) was added to initiate the measurement. The final volume was 100 μl. The reaction was run at 37°C, with readings taken every 20 s. The initial velocity (relative fluorescence units per minute) was determined as the protease activity of MMP-2.

2.5. Characterization of radiolabeled CTT derivatives

The lipophilicity of ^{111}In-DTPA-CTT and that of [^{125}I]SIB-CTT were estimated by measuring coefficients of partition between 1-octanol and 0.1 M of phosphate buffer (pH 7.0) as follows: a 10-μl aliquot of radiolabeled CTT was mixed with 3 ml each of 1-octanol and 0.1 M of phosphate buffer in a test tube. The mixture was vortexed (3×1 min); it then stood for 20 min. After the procedure had been repeated three times, the mixture was centrifuged for 5 min. Two 1-ml aliquots of each phase were removed, and their radioactivity was measured with a well counter (ARC380CL, Aloka, Tokyo, Japan). The partition coefficient was determined by calculating the ratio of counts per minute to milliliters in 1-octanol to that in buffer and then expressed as a common logarithm (log PC).

The molecular charges of the three ^{111}In-DTPA-conjugated CTT derivatives were determined by cellulose acetate electrophoresis. Cellulose acetate strips (Separax-SP, Jokoh, Tokyo, Japan) were run in 20 mM of phosphate buffer (pH 7.4) at a constant current of 0.8 mA/cm for 40 min.

2.6. Serum stability of ^{111}In-DTPA-CTT

^{111}In-DTPA-CTT was diluted 10-fold with murine serum, and the solution was incubated at 37°C for 3 h. The radioactivity of the sample was analyzed by reversed-phase HPLC, TLC and cellulose acetate electrophoresis after

filtering through a 10-kDa cutoff ultrafiltration membrane (Microcon-10, Amicon, Beverly, MA, USA).

2.7. Biodistribution experiments

Animal experiments were conducted in accordance to our institutional guidelines, and the experimental procedures were approved by the Kyoto University Animal Care Committee. Tumor-bearing mice were prepared by implantation of human breast cancer cells (MDA-MB-231 or MDA-MB-435S) into the mammary fat pad of female BALB/c nude mice. When tumors were palpable, about 5 mm in diameter, the mice were used for biodistribution experiments. Biodistribution experiments were performed by intravenously administering radiolabeled peptides (8–30 kBq, <150 ng of peptide) to normal mice (6-week-old male ddY mice, 27–30 g) or tumor-bearing mice. At selected time points after dosing, mice were killed by decapitation and aliquots of blood were collected. Tissues of interest were excised and weighed, and their radioactivity was measured with a well counter (ARC380CL). Then, excised tumors were frozen and stored at −70°C.

Frozen tumors were cut into small pieces and homogenized in 0.05 M of Tris–HCl buffer (pH 7.5) containing 0.2 M of NaCl, 5 mM of $CaCl_2$ and 0.1% Triton X-100. After centrifugation at 8000×*g* for 10 min at 4°C, the supernatant was assayed for gelatinase. Gelatinase activity was measured with a commercially available assay kit (Chemicon, Temicula, CA, USA) according to the manufacturer's instructions.

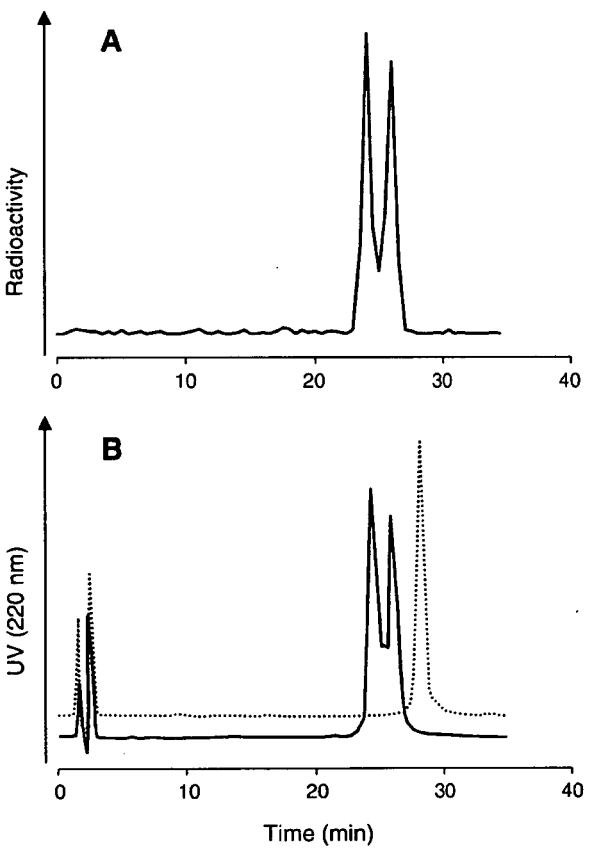

Fig. 2. Analytical HPLC profiles of ^{111}In-DTPA-CTT (A) and nonradioactive In-DTPA-CTT (B). The dotted line represents the profile of DTPA-CTT.

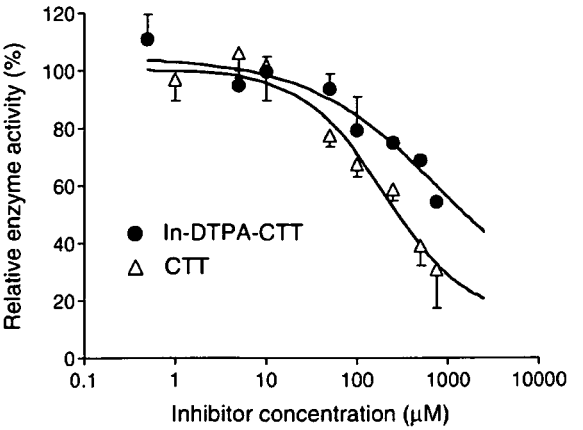

Fig. 3. Inhibition of the proteolytic activity of MMP-2 by In-DTPA-CTT and CTT. Each value represents the mean±S.D. of three experiments.

2.8. Statistical analysis

Data are expressed as means±standard deviations where appropriate. Results were analyzed using the unpaired *t* test. Differences were considered to be statistically significant when *P* values were lower than .05.

3. Results

3.1. Synthesis

Radiochemical purities of all the radiolabeled CTT derivatives exceeded 95% as determined by HPLC and TLC. Specific activities of all peptides were over 400 GBq/mmol. In the HPLC analysis, all three ^{111}In-DTPA-

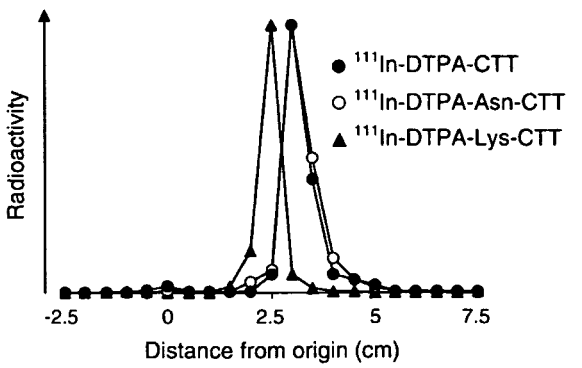

Fig. 4. Radioactivity profiles of ^{111}In-DTPA-conjugated CTT derivatives on cellulose acetate electrophoresis.

Table 1
Biodistribution of radioactivity after the injection of ^{111}In-DTPA-CTT in normal mice

	Time after injection					
	10 min	30 min	1 h	3 h	6 h	24 h
Blood[a]	2.50±0.40	0.61±0.20	0.26±0.03	0.18±0.04	0.18±0.07	0.09±0.03
Liver[a]	1.51±0.40	0.94±0.49	0.83±0.13	0.70±0.25	0.81±0.34	0.40±0.14
Kidney[a]	13.48±2.03	8.34±1.93	7.83±1.09	5.52±0.75	4.66±0.50	2.93±0.76
Intestine[a]	0.53±0.10	0.21±0.10	0.18±0.10	0.33±0.29	0.44±0.13	0.16±0.09
Spleen[a]	1.30±0.39	0.79±0.48	0.67±0.18	0.51±0.10	0.64±0.41	0.38±0.16
Lung[a]	1.96±0.36	0.40±0.07	0.21±0.06	0.12±0.03	0.11±0.03	0.07±0.02
Heart[a]	0.83±0.18	0.20±0.06	0.09±0.03	0.07±0.03	0.10±0.06	0.07±0.01
Feces[b]						2.65±1.90
Urine[b]						69.50±6.83

Each value represents the mean±S.D. of at least five experiments.
[a] Expressed as percent injected dose per gram of organ.
[b] Expressed as percent injected dose.

conjugated CTTs showed two peaks. A typical chromatogram of ^{111}In-DTPA-CTT is depicted in Fig. 2A. Non-radioactive In-DTPA-CTT also showed two peaks at retention times of 26 and 28 min (Fig. 2B), and the IS-MS of both components showed a peak at *m/z* 1653.5 in the positive ion mode. Reanalysis of each isolated component (26 or 28 min) showed two peaks at retention times of 26 and 28 min, indicating that In-DTPA-CTT eluted as well-separated isomers under the analytical conditions. Similar findings were observed with other In-DTPA-conjugated peptides [16,22,23].

3.2. MMP-2 inhibition assay

The inhibitory activity of ^{111}In-DTPA-CTT toward MMP-2 was examined to elucidate the validity of the introduction of ^{111}In-DTPA into an N-terminal residue distant from the HWGF motif. As shown in Fig. 3, In-DTPA-CTT inhibited the proteolytic activity of MMP-2 in a concentration-dependent fashion with an IC_{50} of 1026 μM, although the inhibitory activity was slightly weaker than that of the mother compound (283 μM).

3.3. Characterization of radiolabeled CTT derivatives

The partition coefficients (log PC) of ^{111}In-DTPA-CTT and [^{125}I]SIB-CTT were determined to be −4.0 and 1.1, respectively.

Fig. 4 illustrates the radioactivity profiles of ^{111}In-DTPA-conjugated CTT derivatives on cellulose acetate electrophoresis. ^{111}In-DTPA-CTT and ^{111}In-DTPA-Asn-CTT were detected at the same distance from the origin. On the other hand, ^{111}In-DTPA-Lys-CTT migrated toward the cathode as compared with ^{111}In-DTPA-CTT.

3.4. Serum stability

After incubation in murine serum at 37°C for 3 h, about 85% of the radioactivity was observed in fractions of ^{111}In-DTPA-CTT.

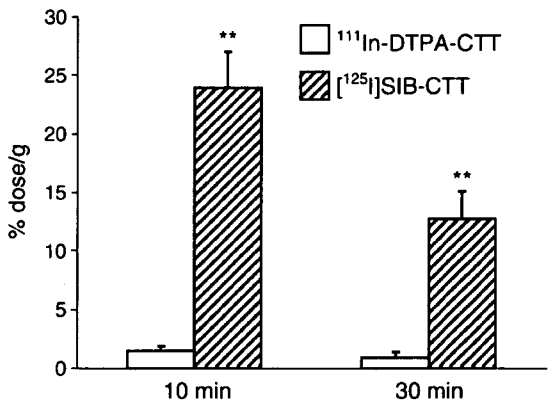

Fig. 5. Hepatic radioactivity levels 10 and 30 min after the injection of ^{111}In-DTPA-CTT or [^{125}I]SIB-CTT in normal mice. Each value represents the mean±S.D. of at least five experiments. **Significant difference from ^{111}In-DTPA-CTT, $P<.0001$.

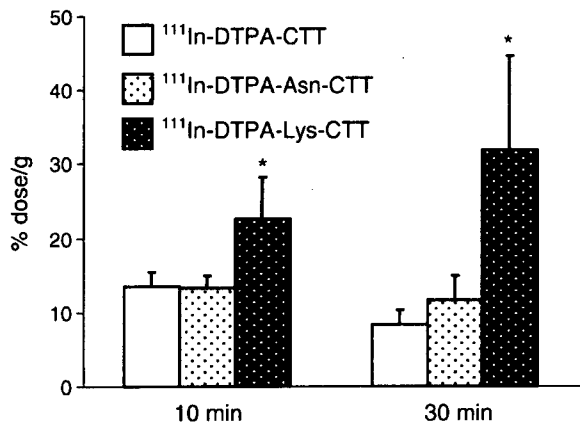

Fig. 6. Renal radioactivity levels 10 and 30 min after the injection of ^{111}In-DTPA-conjugated CTT derivatives in normal mice. Each value represents the mean±S.D. of at least five experiments. *Significant difference from ^{111}In-DTPA-CTT, $P<.005$.

Table 2
Biodistribution of radioactivity after the injection of ^{111}In-DTPA-CTT in mice bearing human breast carcinoma (MDA-MB-231 or MDA-MB-435S) xenografts

	MDA-MB-231			MDA-MB-435S		
	30 min	1 h	3 h	30 min	1 h	3 h
Blood[a]	0.56±0.14	0.22±0.11	0.09±0.01	0.91±0.25	0.37±0.09	0.16±0.04
Liver[a]	0.28±0.05	0.16±0.01	0.12±0.02	0.44±0.06	0.31±0.04	0.23±0.03
Kidney[a]	7.80±0.57	8.04±0.66	8.19±1.23	10.8±1.51	8.14±1.47	7.80±1.15
Muscle[a]	0.11±0.04	0.03±0.02	0.01±0.01	0.17±0.05	0.04±0.02	0.00±0.01
Tumor[a]	0.44±0.16	0.25±0.11	0.24±0.05	0.50±0.16	0.42±0.17	0.13±0.08
Tumor-to-blood ratio	0.78±0.19	1.06±0.24	2.81±0.89	0.54±0.06	1.11±0.33	0.94±0.18

Each value represents the mean±S.D. of four or five experiments.
[a] Expressed as percent injected dose per gram of organ.

3.5. Biodistribution experiments

The biodistribution of radioactivity after intravenous injection of ^{111}In-DTPA-CTT in normal mice is summarized in Table 1. ^{111}In-DTPA-CTT showed rapid clearance from the circulation. The hepatic accumulation of the radioactivity was low (below ~2% injected dose/g), and the majority of the radioactivity was excreted via the kidneys into urine.

Fig. 5 shows hepatic levels of radioactivity after the injection of ^{111}In-DTPA-CTT and [^{125}I]SIB-CTT. [^{125}I]SIB-CTT demonstrated marked accumulation in the liver as compared with ^{111}In-DTPA-CTT.

Renal levels of radioactivity of three ^{111}In-DTPA-conjugated CTT derivatives are shown in Fig. 6. While ^{111}In-DTPA-Asn-CTT accumulated similarly to ^{111}In-DTPA-CTT, ^{111}In-DTPA-Lys-CTT exhibited the highest level early postinjection.

The biodistribution of ^{111}In-DTPA-CTT in tumor-bearing mice is summarized in Table 2. ^{111}In-DTPA-CTT showed greater accumulation in the tumor than in the blood and muscle in the MDA-MB-231-bearing mice. Between the accumulation in the tumor as well as tumor-to-blood ratio and gelatinase activity, a significant correlation was observed (Fig. 7).

4. Discussion

The regulation of MMP activity occurs at several levels, including gene transcriptional control, proenzyme activation and inhibition of activated enzymes by endogenous inhibitors [1,2]. Thus, specific endogenous inhibitors, tissue inhibitors of metalloproteinases (TIMPs), were initially considered as anticancer agents [24,25]. Thereafter, a number of synthetic inhibitors were developed and widely tested in clinical trials [10–12].

In nuclear medicine, a radiolabeled TIMP derivative was, to our knowledge, the first compound to be evaluated for imaging MMP expression [26,27]. Recently, some radiolabeled synthetic MMP inhibitors were studied [28–35]. However, they showed marked accumulation in nontarget tissues in biodistribution studies. Thus, the basic requirements for a radiolabeled MMP inhibitor peptide for the imaging of tumors include good inhibitory activity and selectivity for MMPs, high accumulation in the tumor and low accumulation in nontumor tissues. Taking into account these factors, in the present study, we selected a gelatinase-selective inhibitor with strong inhibitory activity, CTT peptide, as the mother compound and designed a radiolabeled CTT peptide (^{111}In-DTPA-CTT) to reduce the

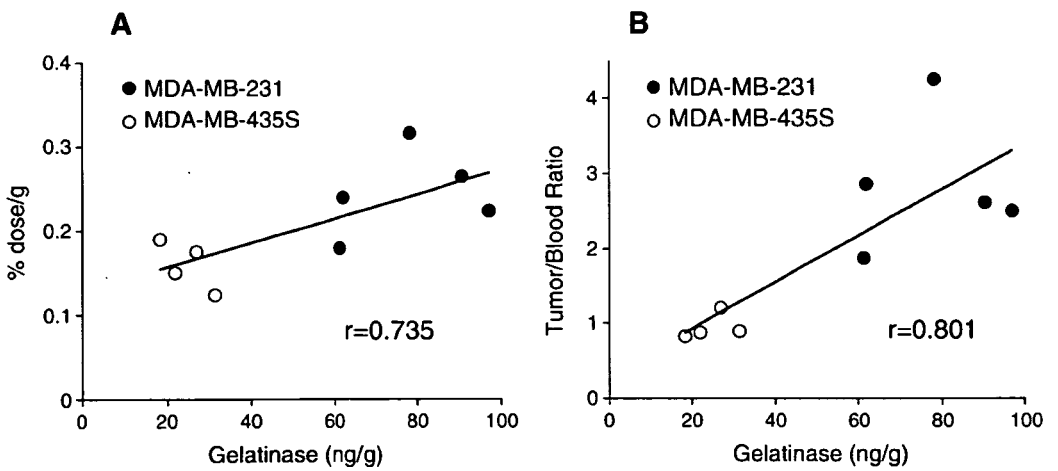

Fig. 7. Correlation between the accumulation in the tumor (A) and tumor-to-blood ratio (B) of ^{111}In-DTPA-CTT 3 h after injection and gelatinase activity. The correlation coefficients (r) were 0.735 and 0.801, respectively.

accumulation in nontarget tissues without impairing inhibitory activity.

An N-terminal residue distant from the motif (HWGF) important for the inhibitory activity of CTT was selected as a radiolabeling site. In addition, ^{111}In-DTPA labeling was adopted as a radiolabeling method for reasons outlined below, and DTPA was attached to the N-terminus of CTT. MMPs possess zinc ions in the catalytic domain [36,37], and so there is a possibility that free chelators such as DTPA-CTT inhibit the MMP activity. Thus, nonradioactive In-DTPA-CTT was prepared and the effect of the conjugation of ^{111}In-DTPA on the inhibition of gelatinase was investigated (Fig. 2). In-DTPA-CTT inhibited the proteolytic activity of MMP-2 in a concentration-dependent fashion, although the inhibitory effect was slightly weaker than that of the mother compound (Fig. 3). This result demonstrates that conjugation of In-DTPA chelate with the N-terminal residue would not cause a marked decrease in the inhibitory activity of CTT. Recently, Li and Anderson [34] pointed out the possibility that gelatinase activity could be imaged with radiolabeled CTT peptides. Thus, radiolabeled CTT peptides should be potential candidates for the imaging of gelatinase activity in tumors.

Peptide-based radiopharmaceuticals are useful for diagnostic applications due to their high affinity and selectivity for target molecules, but an accumulation of radioactivity has been observed in nontarget tissues such as the liver and kidney, thus resulting in a high background of radioactivity [15]. In this study, a highly hydrophilic and negatively charged ^{111}In-chelate, ^{111}In-DTPA, was attached to the amino group of the CTT peptide to reduce accumulation in the liver and kidney. As expected, ^{111}In-DTPA-CTT exhibited low levels of radioactivity in the murine liver (Table 1). Furthermore, renal levels were also found to be low as compared with those of other ^{111}In-DTPA-labeled peptides [17,23]. The hepatic and renal accumulations of ^{111}In-DTPA-CTT were compared with those of other radiolabeled CTT derivatives to validate the chemical design. Comparison with the radioiodinated derivative [^{125}I]SIB-CTT revealed that the conjugation with ^{111}In-DTPA increased the hydrophilicity of the CTT peptide and reduced accumulation in the liver (Fig. 6). Furthermore, a basic (lysine) or neutral (asparagine) amino acid was attached to the N-terminus of CTT to investigate the effect of molecular charge on the renal accumulation of ^{111}In-DTPA-conjugated CTT peptides (Fig. 1). Cellulose acetate electrophoresis indicated that ^{111}In-DTPA-CTT and ^{111}In-DTPA-Asn-CTT had similar net charges and that ^{111}In-DTPA-Lys-CTT had a more positive charge (Fig. 4). When injected into mice, there was no significant difference in renal accumulation between ^{111}In-DTPA-CTT and ^{111}In-DTPA-Asn-CTT. ^{111}In-DTPA-Lys-CTT, on the other hand, showed a significantly higher uptake in the kidney than did ^{111}In-DTPA-CTT. These findings indicate that the conjugation of ^{111}In-DTPA with the amino group of the CTT peptide significantly altered the net molecular charge of the peptide, leading to a significant effect on the renal accumulation.

In MDA-MB-231 tumor-bearing mice, ^{111}In-DTPA-CTT showed greater accumulation in the tumor and tumor-to-blood ratio 3 h after the injection as compared with that in MDA-MB-435S tumor-bearing mice (Table 2). Since the gelatinase activity of the MDA-MB-231 tumor was significantly stronger than that of the MDA-MB-435S tumor (61.3±21.3 and 17.8±6.6, respectively), the accumulation in the tumor might be implicated in the gelatinase activity. Furthermore, the accumulation in the tumor as well as tumor-to-blood ratio 3 h after the injection correlated well with gelatinase activity (Fig. 7). These results demonstrate the feasibility of imaging gelatinase activity in tumors in vivo using ^{111}In-DTPA-CTT. However, the relatively low tumor contrast emphasizes the need for further investigation of the molecular interactions between the peptidic inhibitor and the gelatinase enzyme.

In conclusion, a peptidic gelatinase-selective inhibitor, CTT, was selected as a mother compound and ^{111}In-DTPA-CTT was designed to reduce the accumulation in nontarget tissues and maintain the inhibitory activity, taking into consideration the HWGF motif of the peptide, hydrophilicity and negative charge. In-DTPA-CTT significantly inhibited the proteolytic activity of MMP-2. When injected into normal mice, ^{111}In-DTPA-CTT showed low levels of radioactivity in nontarget tissues such as the liver and kidney. Furthermore, in tumor-bearing mice, ^{111}In-DTPA-CTT showed tumor accumulation that might be implicated in gelatinase activity. Therefore, the conjugation of ^{111}In-DTPA to the N-terminal of CTT would be a promising design for imaging gelatinase activity. Although more studies on the imaging of gelatinase activity in vivo are needed, these findings provide useful information about the chemical design of CTT peptide-based radiopharmaceuticals.

Acknowledgments

This work was supported in part by a Grant-in-Aid for Cancer Research from the Ministry of Health, Labor and Welfare, a grant from the Clinical Research Foundation (2004), a research grant from the Kimura Memorial Heart Foundation (2004), a grant from the Shimadzu Science Foundation and the research fund of the Kyushu University Foundation.

We thank Nihon Medi-Physics for kindly providing $^{111}InCl_3$.

References

[1] Nagase H, Woessner Jr JF. Matrix metalloproteinases. J Biol Chem 1999;274:21491–4.

[2] Sternlicht MD, Werb Z. How matrix metalloproteinases regulate cell behavior. Annu Rev Cell Dev Biol 2001;17:463–516.

[3] Kleiner DE, Stetler-Stevenson WG. Matrix metalloproteinases and metastasis. Cancer Chemother Pharmacol 1999;43:S42–51.

[4] Nelson AR, Fingleton B, Rothenberg ML, Matrisian LM. Matrix metalloproteinases: biologic activity and clinical implications. J Clin Oncol 2000;18:1135–49.
[5] John A, Tuszynski G. The role of matrix metalloproteinases in tumor angiogenesis and tumor metastasis. Pathol Oncol Res 2001;7:14–23.
[6] Di Nezza LA, Misajon A, Zhang J, Jobling T, Quinn MA, Östör AG, et al. Presence of active gelatinases in endometrial carcinoma and correlation of matrix metalloproteinase expression with increasing tumor grade and invasion. Cancer 2002;94:1466–75.
[7] Hrabec E, Strek M, Nowak D, Greger J, Suwalski M, Hrabec Z. Activity of type IV collagenases (MMP-2 and MMP-9) in primary pulmonary carcinomas: a quantitative analysis. J Cancer Res Clin Oncol 2002;128:197–204.
[8] Waas ET, Lomme RM, DeGroot J, Wobbes T, Hendriks T. Tissue levels of active matrix metalloproteinase-2 and -9 in colorectal cancer. Br J Cancer 2002;86:1876–83.
[9] Edwards JG, McLaren J, Jones JL, Waller DA, O'Byrne KJ. Matrix metalloproteinases 2 and 9 (gelatinases A and B) expression in malignant mesothelioma and benign pleura. Br J Cancer 2003;88: 1553–9.
[10] Whittaker M, Floyd CD, Brown P, Gearing AJ. Design and therapeutic application of matrix metalloproteinase inhibitors. Chem Rev 1999; 99:2735–76.
[11] Hidalgo M, Eckhardt SG. Development of matrix metalloproteinase inhibitors in cancer therapy. J Natl Cancer Inst 2001;93:178–93.
[12] Coussens LM, Fingleton B, Matrisian LM. Matrix metalloproteinase inhibitors and cancer: trials and tribulations. Science 2002;295: 2387–92.
[13] Koivunen E, Arap W, Valtanen H, Rainisalo A, Medina OP, Heikkilä P, et al. Tumor targeting with a selective gelatinase inhibitor. Nat Biotechnol 1999;17:768–74.
[14] Okarvi SM. Peptide-based radiopharmaceuticals: future tools for diagnostic imaging of cancers and other diseases. Med Res Rev 2004;24:357–97.
[15] Krenning EP, Kwekkeboom DJ, Bakker WH, Breeman WAP, Kooij PPM, Oei HY, et al. Somatostatin receptor scintigraphy with [^{111}In-DTPA-D-Phe^{1}]- and [^{123}I-Tyr^{3}]-octreotide: the Rotterdam experience with more than 1000 patients. Eur J Nucl Med 1993;20:716–31.
[16] van Hagen PM, Breeman WAP, Bernard HF, Schaar M, Mooij CM, Srinivasan A, et al. Evaluation of a radiolabelled cyclic DTPA-RGD analogue for tumour imaging and radionuclide therapy. Int J Cancer 2000;90:186–98.
[17] Akizawa H, Arano Y, Mifune M, Iwado A, Saito Y, Mukai T, et al. Effect of molecular charges on renal uptake of ^{111}In-DTPA-conjugated peptides. Nucl Med Biol 2001;28:761–8.
[18] Akizawa H, Takimoto H, Saito M, Iwado A, Mifune M, Saito Y, et al. Effect of carboxylation of N-terminal phenylalanine of ^{111}In-DTPA (diethylenetriaminepentaacetic acid)-octreotide on accumulation of radioactivity in kidney. Biol Pharm Bull 2004;27:271–2.
[19] Arano Y, Uezono T, Akizawa H, Ono M, Wakisaka K, Nakayama M, et al. Reassessment of diethylenetriaminepentaacetic acid (DTPA) as a chelating agent for indium-111 labeling of polypeptides using a newly synthesized monoreactive DTPA derivative. J Med Chem 1996;39: 3451–60.
[20] Arano Y, Wakisaka K, Ohmomo Y, Uezono T, Mukai T, Motonari H, et al. Maleimidoethyl 3-(tri-n-butylstannyl)hippurate: a useful radioiodination reagent for protein radiopharmaceuticals to enhance target selective radioactivity localization. J Med Chem 1994;37:2609–18.
[21] Arano Y, Akizawa H, Uezono T, Akaji K, Ono M, Funakoshi S, et al. Conventional and high-yield synthesis of DTPA-conjugated peptides: application of a monoreactive DTPA to DTPA-D-Phe^{1}-octreotide synthesis. Bioconjug Chem 1997;8:442–6.
[22] Albert R, Miller K, Chong R, Hirth W, Vanderheyden J-L, Deutsch K, et al. Characterization of the two diastereomers of octreoscan-111, an In-111 labeled peptide for use in cancer imaging. J Nucl Med 1992;33: 900 [abstract].
[23] Akizawa H, Arano Y, Mifune M, Iwado A, Saito Y, Uehara T, et al. Significance of ^{111}In-DTPA chelate in renal radioactivity levels of ^{111}In-DTPA-conjugated peptides. Nucl Med Biol 2001;28:459–68.
[24] Schultz RM, Silberman S, Persky B, Bajkowski AS, Carmichael DF. Inhibition by human recombinant tissue inhibitor of metalloproteinases of human amnion invasion and lung colonization by murine B16-F10 melanoma cells. Cancer Res 1988;48:5539–45.
[25] Alvarez OA, Carmichael DF, DeClerck YA. Inhibition of collagenolytic activity and metastasis of tumor cells by a recombinant human tissue inhibitor of metalloproteinases. J Natl Cancer Inst 1990;82:589–95.
[26] Giersing BK, Rae MT, CarballidoBrea M, Williamson RA, Blower PJ. Synthesis and characterization of ^{111}In-DTPA-N-TIMP-2: a radiopharmaceutical for imaging matrix metalloproteinase expression. Bioconjug Chem 2001;12:964–71.
[27] Kulasegaram R, Giersing B, Page CJ, Blower PJ, Williamson RA, Peters BS, et al. In vivo evaluation of ^{111}In-DTPA-N-TIMP-2 in Kaposi sarcoma associated with HIV infection. Eur J Nucl Med 2001;28: 756–61.
[28] Furumoto S, Iwata R, Ido T. Design and synthesis of fluorine-18 labeled matrix metalloproteinase inhibitor for cancer imaging. J Labelled Compd Radiopharm 2002;45:975–86.
[29] Zheng Q-H, Fei X, Liu X, Wang J-Q, Sun HB, Mock BH, et al. Synthesis and preliminary biological evaluation of MMP inhibitor radiotracers [^{11}C]methyl-halo-CGS 27023A analogs, new potential PET breast cancer imaging agents. Nucl Med Biol 2002;29:761–70.
[30] Furumoto S, Takashima K, Kubota K, Ido T, Iwata R, Fukuda H. Tumor detection using ^{18}F-labeled matrix metalloproteinase-2 inhibitor. Nucl Med Biol 2003;30:119–25.
[31] Zheng Q-H, Fei X, DeGrado TR, Wang J-Q, Stone KL, Martinez TD, et al. Synthesis, biodistribution and micro-PET imaging of a potential cancer biomarker carbon-11 labeled MMP inhibitor (2R)-2-[[4-(6-fluorohex-1-ynyl)phenyl]sulfonylamino]-3-methylbutyric acid [^{11}C] methyl ester. Nucl Med Biol 2003;30:753–60.
[32] Kuhnast B, Bodenstein C, Wester HJ, Weber W. Carbon-11 labelling of an N-sulfonylamino acid derivative: a potential tracer for MMP-2 and MMP-9 imaging. J Labelled Compd Radiopharm 2003;46:539–53.
[33] Zheng Q-H, Fei X, Liu X, Wang J-Q, Stone KL, Martinez TD, et al. Comparative studies of potential cancer biomarkers carbon-11 labeled MMP inhibitors (*S*)-2- (4′-[^{11}C]methoxybiphenyl-4-sulfonylamino)-3-methylbutyric acid and N-hydroxy-(*R*)-2-[[(4′-[^{11}C]methoxyphenyl) sulfonyl]benzylamino]-3-methylbutanamide. Nucl Med Biol 2004;31: 77–85.
[34] Li WP, Anderson CJ. Imaging matrix metalloproteinase expression in tumors. Q J Nucl Med 2003;47:201–8.
[35] Kuhnast B, Bodenstein C, Haubner R, Wester HJ, Senekowitsch-Schmidtke R, Schwaiger M, et al. Targeting of gelatinase activity with a radiolabeled cyclic HWGF peptide. Nucl Med Biol 2004;31:337–44.
[36] Van H, Wart E, Birkedal-Hansen H. The cysteine switch: a principle of regulation of metalloproteinase activity with potential applicability to the entire matrix metalloproteinase gene family. Proc Natl Acad Sci U S A 1990;87:5578–82.
[37] Morgunova E, Tuuttila A, Bergmann U, Isupov M, Lindqvist Y, Schneider G, et al. Structure of human pro-matrix metalloproteinase-2: activation mechanism revealed. Science 1999;284:1667–70.

Usefulness of ^{11}C-Methionine for Differentiating Tumors from Granulomas in Experimental Rat Models: A Comparison with ^{18}F-FDG and ^{18}F-FLT

Songji Zhao[1], Yuji Kuge[2,3], Masashi Kohanawa[4], Toshiyuki Takahashi[5], Yan Zhao[1], Min Yi[4], Kakuko Kanegae[1], Koh-ichi Seki[6], and Nagara Tamaki[1]

[1]Department of Nuclear Medicine, Graduate School of Medicine, Hokkaido University, Sapporo, Japan; [2]Department of Molecular Imaging, Graduate School of Medicine, Hokkaido University, Sapporo, Japan; [3]Department of Patho-Functional Bioanalysis, Graduate School of Pharmaceutical Sciences, Kyoto University, Kyoto, Japan; [4]Department of Microbiology, Graduate School of Medicine, Hokkaido University, Sapporo, Japan; [5]Department of Pathology, Hokkaido Gastroenterology Hospital, Sapporo, Japan; and [6]Central Institute of Isotope Science, Hokkaido University, Sapporo, Japan

Many clinical PET studies have shown that increased ^{18}F-FDG uptake is not specific to malignant tumors. ^{18}F-FDG is also taken up in inflammatory lesions, particularly in granulomatous lesions such as sarcoidosis or active inflammatory processes after chemoradiotherapy, making it difficult to differentiate malignant tumors from benign lesions, and is the main source of false-positive ^{18}F-FDG PET findings in oncology. These problems may be overcome by multitracer studies using 3′-deoxy-3′-^{18}F-fluorothymidine (^{18}F-FLT) or L-^{11}C-methionine. However, ^{18}F-FLT or ^{11}C-methionine uptake in granulomatous lesions remains unclarified. In this study, the potentials of ^{18}F-FLT and ^{11}C-methionine in differentiating malignant tumors from granulomas were compared with ^{18}F-FDG using experimental rat models. **Methods:** Dual-tracer tissue distribution studies using ^{18}F-FDG and ^{3}H-FLT (groups I and III) or ^{18}F-FDG and ^{14}C-methionine (groups II and IV) were performed on rats bearing both granulomas (*Mycobacterium bovis* bacillus Calmette-Guérin [BCG]–induced) and hepatomas (KDH-8–induced) (groups I and II) or on rats bearing both turpentine oil–induced inflammation and hepatomas (groups III and IV). One hour after the injection of a mixture of ^{18}F-FDG and ^{3}H-FLT or of ^{18}F-FDG and ^{14}C-methionine, tissues were excised to determine the radioactivities of ^{18}F-FDG, ^{3}H-FLT, and ^{14}C-methionine (differential uptake ratio). **Results:** Mature epithelioid cell granuloma formation and massive lymphocyte infiltration were observed in the granuloma tissue induced by BCG, histologically similar to sarcoidosis. The granulomas showed high ^{18}F-FDG uptake comparable to that in the hepatomas (group I, 8.18 ± 2.40 vs. 9.13 ± 1.52, P = NS; group II, 8.43 ± 1.45 vs. 8.91 ± 2.32, P = NS). ^{14}C-Methionine uptake in the granuloma was significantly lower than that in the hepatoma (1.31 ± 0.22 vs. 2.47 ± 0.60, $P < 0.01$), whereas ^{3}H-FLT uptake in the granuloma was comparable to that in the hepatoma (1.98 ± 0.70 vs. 2.30 ± 0.67, P = NS). Mean uptake of ^{18}F-FDG, ^{3}H-FLT, and ^{14}C-methionine was markedly lower in the turpentine oil–induced inflammation than in the tumor. **Conclusion:** ^{14}C-Methionine uptake was significantly lower in the granuloma than in the tumor, whereas ^{18}F-FDG and ^{3}H-FLT were not able to differentiate granulomas from tumors. These results suggest that ^{14}C-methionine has the potential to accurately differentiate malignant tumors from benign lesions, particularly granulomatous lesions, providing a biologic basis for clinical PET studies.

Key Words: ^{11}C-methionine; granuloma; inflammation; tumor; rat

J Nucl Med 2008; 49:135–141
DOI: 10.2967/jnumed.107.044578

As a useful tracer for tumor imaging with PET, ^{18}F-FDG has been widely applied to tumor detection, staging, evaluation of treatment response, and differentiation of malignant tumors from benign lesions in clinical oncology (*1,2*). These applications are based on the increased ^{18}F-FDG uptake due to enhanced glucose use in most tumors. Recent investigations, including many clinical PET studies, however, have shown that increased ^{18}F-FDG uptake is not specific to malignant tumors (*3–7*). ^{18}F-FDG is also taken up in inflammatory lesions, particularly in granulomatous lesions such as sarcoidosis or active inflammatory processes after chemoradiotherapy (*3–7*), making it difficult to differentiate malignant tumors from benign lesions, and is the main source of false-positive ^{18}F-FDG PET findings in oncology (*8*). It has been suggested that these problems may be overcome by multitracer studies using 3′-deoxy-3′-^{18}F-fluorothymidine (^{18}F-FLT) or L-^{11}C-methionine (*8,9*).

^{18}F-FLT, a radiolabeled analog of thymidine, has been developed as a PET tracer to image cellular proliferation in vivo (*10*). ^{18}F-FLT is phosphorylated by the enzyme thymidine kinase 1, which leads to intracellular trapping of the tracer. During DNA synthesis, thymidine kinase 1 activity increases almost 10-fold and is thus an accurate reflection of cellular proliferation (*8,11*). On the other hand, ^{11}C-methionine

Received Jun. 25, 2007; revision accepted Sep. 18, 2007.
For correspondence or reprints contact: Nagara Tamaki, MD, PhD, Department of Nuclear Medicine, Graduate School of Medicine, Hokkaido University, Kita 15 Nishi 7, Kita-ku, Sapporo 060-8638, Japan.
E-mail: natamaki@med.hokudai.ac.jp

uptake reflects increased amino acid transport and protein synthesis and is related to cellular proliferation. ^{11}C-Methionine has been shown to possess a high specificity in tumor detection, tumor delineation, and differentiation of benign from malignant lesions (*12,13*) because of the lower uptake of ^{11}C-methionine than of ^{18}F-FDG in inflammatory cells (*14–16*). These factors suggest that thymidine or amino acid tracers are potentially more suitable than ^{18}F-FDG for the differentiation of tumors from inflammatory lesions. However, the uptake of these tracers in granulomatous lesions remains unclarified, mainly because of the lack of suitable animal models. In this regard, we have recently developed a rat model of intramuscular granuloma characterized by epithelioid cell granuloma formation and massive lymphocyte infiltration around the granuloma, histologically similar to sarcoidosis (*17*). The rat granuloma showed high ^{18}F-FDG uptake comparable to that in the tumor, indicating the usefulness of our model for studies of differential diagnosis.

The purpose of this study was to compare the potentials of ^{18}F-FLT and ^{11}C-methionine with ^{18}F-FDG for differentiating malignant tumors from granulomas in the rat model bearing granuloma and tumor.

MATERIALS AND METHODS

Radiopharmaceuticals

^{18}F-FDG, synthesized by standard procedures, was obtained from Hokkaido University Hospital Cyclotron Facility. L-[methyl-^{14}C]methionine (specific activity, 1.48–2.04 GBq/mmol) and [methyl-^{3}H (N)]-3′-fluoro 3′-deoxythymidine (^{3}H-FLT) (specific activity, 74–370 GBq/mmol) were purchased from American Radiolabeled Chemicals, Inc., and Moravek Biochemicals Inc.

Animal Studies

All experimental protocols were approved by the Laboratory Animal Care and Use Committee of Hokkaido University. Eight-week-old male Wistar King Aptekman/hok rats (supplied by Japan SLC, Inc.) were used in all experiments. The *Mycobacterium bovis* bacillus Calmette-Guérin (BCG), a Japanese strain, was grown on Middlebrook 7H11 agar (Difco Laboratories), suspended in phosphate-buffered saline with 0.05% polysorbate 20, and stocked at −80°C. BCG (1×10^7 CFU/rat) and allogenic hepatoma cells (KDH-8, 1×10^6 cells/rat) were inoculated, respectively, into the left and right calf muscles to generate a rat model bearing both the granuloma and the tumor. Turpentine oil (0.2 mL/rat) and KDH-8 were inoculated, respectively, into the left and right calf muscles to generate a rat model bearing both turpentine oil–induced inflammation and tumor. Figure 1 shows the experimental protocols of the animal studies. At designated periods after inoculation of KDH-8 and BCG or of KDH-8 and turpentine, the rats were kept fasting overnight, anesthetized with pentobarbital (50 mg/kg of body weight, intraperitoneally), and administered an intravenous injection of a mixture of ^{18}F-FDG (7.4 MBq) and ^{3}H-FLT (0.185 MBq) or of ^{18}F-FDG (7.4 MBq) and ^{14}C-methionine (0.185 MBq). The rats were kept under anesthesia throughout the experiment. To decrease the serum level of endogenous thymidine, the rats were pretreated with thymidine phosphorylase (1,000 U/kg of body weight) 45 min before the injection of a mixture of ^{18}F-FDG and ^{3}H-FLT, according to the procedures reported by van Waarde et al. (*8*). Sixty minutes after the injection of a mixture of ^{18}F-FDG and ^{3}H-FLT or of ^{18}F-FDG and ^{14}C-methionine, the animals were sacrificed, and tumor, granuloma, inflammatory tissues, and other organs were excised. The tissues and blood samples were weighed, and ^{18}F-FDG radioactivity was determined using a γ-counter (1480 WIZARD 3″; Wallac Co., Ltd.). The samples were then solubilized with Soluene 350 (Packard Bioscience B.V.), and ^{3}H-FLT or ^{14}C-methionine radioactivity was measured using a liquid scintillation counter (LSC-5100; Aloka Co., Ltd.). ^{18}F-FDG, ^{3}H-FLT, and ^{14}C-methionine uptake levels in the tissues were expressed as a differential uptake ratio (DUR) (cpm measured per gram of tissue/cpm injected per gram of body weight) (*16*). The lesion (tumor, granuloma, or turpentine-induced inflammatory tissue)-to-muscle (L/M) ratios and the lesion-to-blood (L/B) ratios of ^{18}F-FDG, ^{3}H-FLT, and ^{14}C-methionine uptake were calculated from the DUR value of each tissue (*18,19*). Samples from the tumor, granuloma, and turpentine oil–induced inflammatory tissues were formalin-fixed and paraffin-embedded for the subsequent histologic staining. Blood samples for glucose level measurement were obtained immediately before the tracer injection and immediately before sacrifice. Blood glucose

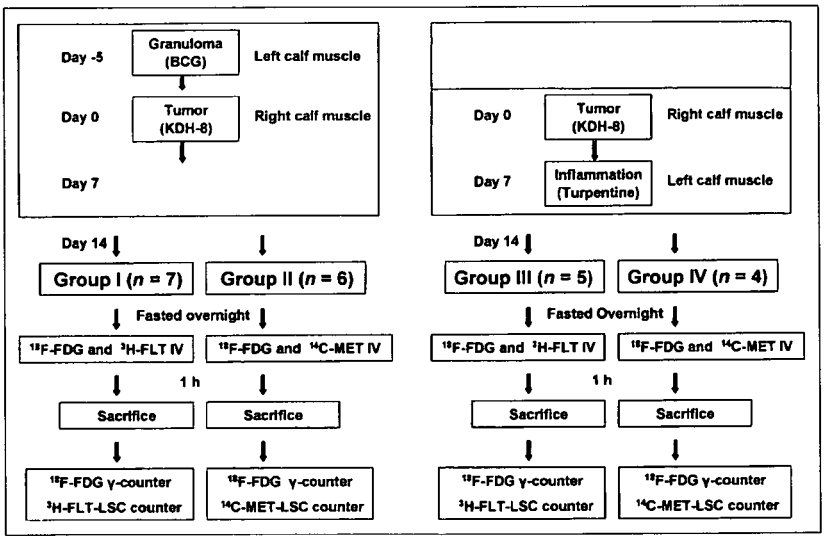

FIGURE 1. Experimental protocols of this study. LSC = liquid scintillation counter.

level was determined using a biochemical analyzer (MediSense; Dainobot Co., Ltd.).

Histochemical Studies

Formalin-fixed, paraffin-embedded 3-μm-thick sections of tumor, granuloma, and turpentine oil–induced inflammation tissue were stained with hematoxylin and eosin. The immunohistochemical staining of an immune-associated antigen (Ia) was also performed using a monoclonal antibody (mAb) (mouse IgG, MRC OX-6; Oxford Biotechnology Ltd.) that recognizes a monomorphic determinant of rat Ia, MHC class II, present on B lymphocytes, dendritic cells, some macrophages, and certain epithelial cells, as previously described (*17*).

Statistical Analysis

All values are expressed as mean ± SD. The nonparametric Kruskal–Wallis test was used to assess the significance of differences in blood glucose levels among the 4 groups of rats. Statistical analyses were performed using a nonparametric Mann–Whitney *U* test to evaluate the significance of differences in values between the 2 types of lesions (tumor vs. granuloma or tumor vs. turpentine-induced inflammation). A value of *P* less than 0.05 was considered significant.

RESULTS

Blood Glucose Level and Histopathologic Findings

There was no statistically significant difference in blood glucose levels among the 4 groups of rats at the times of injection and sacrifice (Table 1). The blood glucose levels were within the physiologic range.

In the intramuscular granuloma induced by BCG, the granulomatous lesions showed mature epithelioid cell granuloma formation and massive lymphocyte infiltration around the granuloma (Fig. 2A). Immunohistochemical staining also showed the accumulation of Ia-positive macrophages and Ia-positive lymphocytes in the periphery of the granuloma (Fig. 2B). In the intramuscular tumor induced by KDH-8 cells, massive viable and proliferating cancer cells were observed by hematoxylin-and-eosin staining (Fig. 2C). In the turpentine-induced inflammatory tissue, massive neutrophil infiltration and ambient connective tissue formation were observed around the site of turpentine oil injection (Fig. 2D).

Uptake of ^{18}F-FDG, ^{3}H-FLT, and ^{14}C-Methionine

^{18}F-FDG, ^{3}H-FLT, and ^{14}C-methionine uptake in the tumor, granuloma, and turpentine-induced inflammatory tissues are summarized in Figure 3 and Table 2.

Figures 3A and 3B show the tracer uptake levels in rats bearing the tumor and granuloma (groups I and II). The granuloma showed high ^{18}F-FDG uptake comparable to that in the tumor (group I, 8.18 ± 2.40 DUR for granuloma vs. 9.13 ± 1.52 DUR for tumor, *P* = NS; group II, 8.43 ± 1.45 DUR for granuloma vs. 8.91 ± 2.32 DUR for tumor, *P* = NS). ^{3}H-FLT uptake in the granuloma was also comparable to that in the tumor (group I, 1.98 ± 0.70 DUR for granuloma vs. 2.30 ± 0.67 DUR for tumor, *P* = NS). Mean ^{14}C-methionine uptake in the granuloma was significantly lower than that in the tumor (group II, 1.31 ± 0.22 DUR for granuloma vs. 2.47 ± 0.60 DUR for tumor, $P < 0.01$). ^{14}C-Methionine uptake in the granuloma was about 53% of that in the tumor (Fig. 3B).

In rats bearing the tumor and turpentine oil–induced inflammatory tissue (Figs. 3C and 3D, groups III and IV), the mean ^{18}F-FDG uptake in the inflammatory tissue was markedly lower than that in the tumor (group III, 2.42 ± 0.43 DUR for inflammatory tissue vs. 9.13 ± 0.50 DUR for tumor, $P < 0.01$; group IV, 3.99 ± 0.22 DUR for inflammatory tissue vs. 11.14 ± 1.03 DUR for tumor, $P < 0.05$). ^{3}H-FLT and ^{14}C-methionine uptake was also significantly lower in the inflammatory tissue than in the tumor (group III, ^{3}H-FLT, 0.99 ± 0.13 DUR for inflammatory tissue vs. 2.66 ± 0.13 DUR for tumor, $P < 0.01$; group IV, ^{14}C-methionine, 1.77 ± 0.18 for inflammatory tissue vs. 2.96 ± 0.57 DUR for tumor, $P < 0.05$).

The L/M and the L/B ratios of ^{18}F-FDG, ^{3}H-FLT, and ^{14}C-methionine uptake are summarized in Table 2. The mean L/M and L/B ratios of ^{18}F-FDG and ^{3}H-FLT uptake in the granuloma were comparable to those in the tumor (group I, *P* = NS). However, the mean L/M and L/B ratios of ^{14}C-methionine uptake in the granuloma was significantly lower than those in the hepatoma (group II, 3.0 ± 0.6 vs. 5.7 ± 1.9 for L/M and 1.8 ± 0.3 vs. 3.5 ± 1.0 for L/B, $P < 0.01$, respectively). The L/M and L/B ratios of ^{18}F-FDG, ^{3}H-FLT, and ^{14}C-methionine uptake in the turpentine-induced inflammation were markedly lower than those in the tumor (groups III and IV).

DISCUSSION

This study showed that ^{14}C-methionine uptake in the granuloma was about 50% of that in the tumor (Fig. 3B), and the difference was significant. In contrast, ^{18}F-FLT and ^{18}F-FDG uptake in the granuloma was comparable to that in

TABLE 1
Blood Glucose Levels (mg/dL)

Time	Group I (*n* = 7): ^{18}F-FDG + ^{3}H-FLT	Group II (*n* = 6): ^{18}F-FDG + ^{14}C-methionine	Group III (*n* = 5): ^{18}F-FDG + ^{3}H-FLT	Group IV (*n* = 4): ^{18}F-FDG + ^{14}C-methionine
At tracer injection	87.7 ± 7.4	93.2 ± 6.5	84.2 ± 8.5	87.3 ± 5.2
At sacrifice	88.0 ± 6.7	86.0 ± 5.7	91.0 ± 8.0	85.3 ± 2.2

Data are mean ± SD.

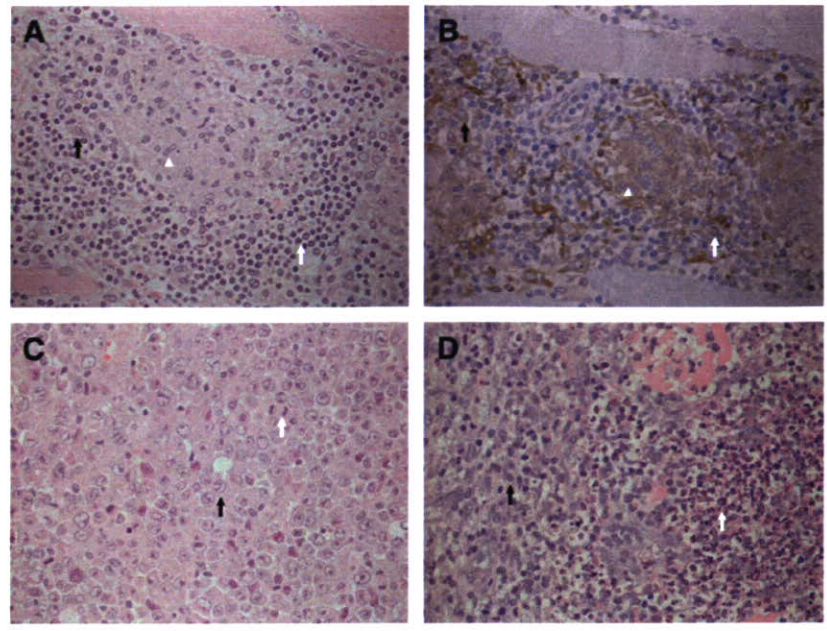

FIGURE 2. Microscopy images (×400) of hematoxylin-and-eosin staining (granuloma [A], tumor [C], and turpentine-induced inflammation [D]) and immunostaining for Ia antigen (granuloma [B]). (A) Intramuscular granuloma induced by BCG shows mature epithelioid cell granuloma formation and massive lymphocyte infiltration around granuloma. (B) Immunostaining for Ia antigen shows infiltrations of Ia-positive epithelioid cells and macrophages in granuloma and Ia-positive lymphocytes in periphery of granuloma. In A and B, arrowhead indicates epithelioid cell granuloma; white arrow, lymphocyte infiltration; and black arrow, macrophage infiltration. (C) Massive viable and proliferating cancer cells in tumor tissue. Black arrow indicates viable cancer cell; white arrow, proliferating cancer cell (mitotic division). (D) Massive neutrophil infiltration and ambient connective tissue formation were observed around site of turpentine oil injection. White arrow indicates neutrophil infiltration; black arrow, connective tissue.

the tumor. These results suggest the possible usefulness of ^{11}C-methionine for differentiating malignant tumors from benign lesions, providing a biologic basis for clinical PET studies.

The present results suggest that amino acid tracers are potentially more suitable than ^{18}F-FDG for the differentiation of tumors from inflammation, including granuloma. Our results are consistent with previous clinical findings that showed that ^{18}F-FDG uptake is significantly higher than ^{11}C-methionine uptake in mediastinal bilateral hilar lymphadenopathy with sarcoidosis (*20*). On the other hand, to the best of our knowledge, this is the first report on radiolabeled ^{14}C-methionine uptake in an experimental granuloma, although studies of ^{14}C-methionine uptake in inflammation induced by intramuscular injections of croton oil and carrageenan (*21*) have been reported.

It is of great importance to determine the cause of the difference between ^{11}C-methionine and ^{18}F-FDG accumulations in granulomas. Cellular uptake of ^{18}F-FDG in sarcoidosis is considered to be related to inflammatory cell infiltrates, which are composed of lymphocytes, macrophages, and epithelioid cells from monocytes, because ^{18}F-FDG has been observed in vitro to be accumulated by leukocytes (*22,23*), lymphocytes, and macrophages (*24*). An increased ^{18}F-FDG distribution level was observed mainly in epithelioid cell granulomas by autoradiography, whereas the ^{14}C-methionine distribution level was low. The activities of granuloma formation and granuloma-associated immune cells may be reflected by the accumulation of ^{18}F-FDG but not by that of ^{14}C-methionine, although the detailed mechanisms underlying the accumulation of these tracers in granulomas remain unclarified. As for the accumulation of these tracers in tumors, Kubota et al. (*15*) have demonstrated by a microautoradiographic study that ^{14}C-methionine uptake is achieved largely by viable cancer cells, whereas uptake by macrophages and granulation tissues is low, in contrast to ^{18}F-FDG. An increased ^{18}F-FDG accumulation in young granulation tissues around a tumor and in macrophages infiltrating the margins of an extensive area of tumor necrosis was observed by microautoradiography using ^{18}F-FDG and ^{3}H-deoxyglucose (*24*). The distinctive uptake profiles of ^{18}F-FDG and ^{11}C-methionine may provide information on the different roles of these tracers in the diagnosis of tumors and inflammation.

This study showed that mean ^{3}F-FLT uptake in the BCG-induced granuloma was comparable to that in the KDH-8–induced hepatoma, as in the case of ^{18}F-FDG, although the level of ^{3}H-FLT uptake was lower than that of ^{18}F-FDG. Some investigators reported that ^{18}F-FLT uptake in inflammatory cells is lower than that in tumors, because the mitotic activity of inflammatory cells is lower than that of tumor cells. Van Waarde et al. reported that ^{18}F-FLT uptake in turpentine-induced inflammation is 32% of that in C6 rat gliomas (*8*), suggesting a high tumor specificity of ^{18}F-FLT (*8*). Our results for turpentine-induced inflammatory tissue were consistent with previous reports. In contrast, ^{3}H-FLT uptake in the granuloma was comparable to that in the hepatoma. Clinical studies (*25*) also showed that a patient with granulomas after radiation and chemotherapy showed increased ^{18}F-FLT uptake. A patient with nonspecific interstitial pneumonia had a false-positive ^{18}F-FLT finding (Ki-67 index, 15%) (*26*). Inflammatory lung diseases are accompanied by lymphocyte infiltration and involve growth factors that enhance the proliferation of lymphocytes (*27*). These findings suggest that ^{18}F-FLT may accumulate in chronic granulomatous lesions with proliferative inflammation. Our

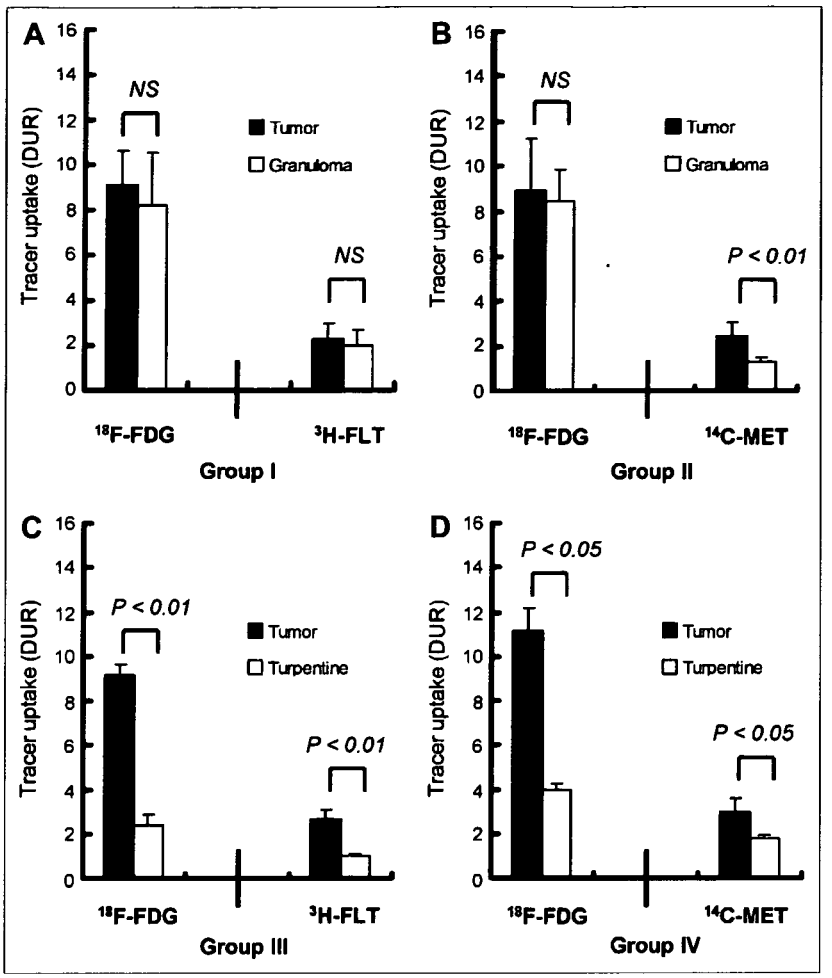

FIGURE 3. ^{18}F-FDG, ^{3}H-FLT, and ^{14}C-methionine uptake in tumor, granuloma, and turpentine oil–induced inflammation. (A) Group I: ^{18}F-FDG and ^{3}H-FLT uptake in tumor and granuloma. (B) Group II: ^{18}F-FDG and ^{14}C-methionine uptake in tumor and granuloma. (C) Group III: ^{18}F-FDG and ^{3}H-FLT uptake in tumor and turpentine oil–induced inflammation. (D) Group IV: ^{18}F-FDG and ^{14}C-methionine uptake in turpentine oil–induced inflammation. Values are mean ± SD. NS = not statistically significant.

study showed the accumulation of Ia-positive lymphocytes in the periphery of the granuloma (Fig. 2B) (Ki-67 index, 6.3%), possibly explaining the increased ^{3}H-FLT uptake in the granulomatous lesions. Thus, our experimental results support previous clinical findings, although detailed investigations, including that of the correlation between the Ki-67 proliferation index and ^{18}F-FLT distribution in the granuloma and tumor using autoradiography, are required.

Although the usefulness of ^{11}C-methionine for differentiating malignant tumors from benign lesions was indicated in our experimental models, uptake of ^{18}F-FLT and ^{11}C-methionine by tumor was relatively lower than uptake of ^{18}F-FDG. An absolute uptake level is also a determinant of the usefulness of radiopharmaceuticals. General tumor detectability might be higher with ^{18}F-FDG than with others, although several clinical and experimental studies suggested that ^{18}F-FDG and ^{11}C-methionine were equally useful in detecting residual or recurrent malignant tumors (*16,28*).

It is important to note the limitations of our study. We measured the biodistribution of ^{14}C-methionine at 60 min after injection, to avoid technical complications. In clinical settings, however, PET images of ^{11}C-methionine are usually acquired at 10–30 min after injection, because of the short half-life of ^{11}C. To investigate whether the biodistribution of ^{14}C-methionine at early time points provides data similar to those of the present study (at 60 min) in differentiating the tumor from the granuloma, we preliminarily performed biodistribution studies at 5, 15, and 30 min after the ^{14}C-methionine injection using the tumor and inflammation models. The findings showed that uptake of ^{14}C-methionine in the tumor and granuloma plateaued at 15–30 min after the injection. ^{14}C-Methionine uptake in the granuloma at 15 and 30 min was also significantly lower than that in the tumor—61% and 45%, respectively, of tumor uptake. These results were consistent with the present results, although ^{14}C-methionine uptake in the tumor and granuloma at 60 min was lower than that at 15 and 30 min. The biodistribution at early time points supports our results in the present study. It should also be noted that uptake of ^{14}C-methionine in normal organs was relatively high in our rats. This result may be ascribed to the time point (60 min after injection) at which we performed the ^{14}C-methionine biodistribution study. Kubota et al. (*29*) reported that the distribution of ^{14}C-methionine in abdominal organs including the liver, intestine, and kidney

TABLE 2
Uptake Levels, L/M, and L/B 60 Minutes After Injection of ^{18}F-FDG, ^{3}H-FLT, and ^{14}C-Methionine (DUR)

	KDH-8 and BCG				KDH-8 and turpentine oil			
	Group I (n = 7)		Group II (n = 6)		Group III (n = 5)		Group IV (n = 4)	
Parameter	^{18}F-FDG	^{3}H-FLT	^{18}F-FDG	^{14}C-Methionine	^{18}F-FDG	^{3}H-FLT	^{18}F-FDG	^{14}C-Methionine
Blood	0.69 ± 0.14	0.91 ± 0.15	0.60 ± 0.11	0.71 ± 0.04	0.57 ± 0.08	0.72 ± 0.11	0.77 ± 0.10	0.99 ± 0.03
Plasma	0.95 ± 0.25	0.85 ± 0.12	0.59 ± 0.13	0.95 ± 0.04	0.66 ± 0.11	0.74 ± 0.08	0.79 ± 0.10	1.37 ± 0.08
Muscle	0.28 ± 0.05	0.85 ± 0.09	0.31 ± 0.11	0.45 ± 0.06	0.20 ± 0.03	0.74 ± 0.07	0.30 ± 0.03	0.41 ± 0.04
Brown fat	0.52 ± 0.48	0.48 ± 0.25	0.33 ± 0.06	0.42 ± 0.07	0.38 ± 0.08	0.43 ± 0.05	0.44 ± 0.03	0.50 ± 0.03
White fat	0.18 ± 0.03	0.16 ± 0.05	0.18 ± 0.02	0.11 ± 0.02	0.21 ± 0.08	0.22 ± 0.09	0.19 ± 0.02	0.13 ± 0.01
Heart	1.04 ± 0.60	0.86 ± 0.10	0.62 ± 0.27	0.83 ± 0.05	0.54 ± 0.05	0.72 ± 0.09	0.60 ± 0.13	0.97 ± 0.03
Brain	3.05 ± 0.24	0.15 ± 0.02	2.97 ± 0.15	0.48 ± 0.03	2.69 ± 0.16	0.16 ± 0.07	3.49 ± 0.46	0.64 ± 0.04
Lung	2.35 ± 0.70	1.51 ± 0.27	1.16 ± 0.13	1.30 ± 0.03	2.51 ± 0.33	1.72 ± 0.25	1.52 ± 0.08	1.63 ± 0.06
Thymus	1.89 ± 0.33	1.03 ± 0.39	2.16 ± 0.23	1.57 ± 0.11	1.20 ± 0.24	0.84 ± 0.46	2.46 ± 0.20	1.85 ± 0.30
Spleen	3.26 ± 0.82	4.20 ± 0.73	2.34 ± 0.26	2.16 ± 0.41	2.75 ± 0.30	5.06 ± 1.09	3.19 ± 0.20	3.03 ± 0.14
Liver	2.37 ± 0.64	1.71 ± 0.34	0.89 ± 0.22	7.15 ± 0.75	2.10 ± 0.40	1.42 ± 0.09	1.24 ± 0.11	7.97 ± 0.83
Kidney	2.06 ± 0.92	2.37 ± 0.38	1.31 ± 0.30	3.76 ± 0.14	1.36 ± 0.24	1.92 ± 0.15	2.98 ± 1.31	3.97 ± 0.23
Bone marrow	2.50 ± 0.35	9.42 ± 0.99	2.37 ± 0.24	3.33 ± 0.24	2.07 ± 0.36	11.93 ± 2.18	2.92 ± 0.14	4.69 ± 0.26
Tumor	9.13 ± 1.52	2.30 ± 0.67	8.91 ± 2.32	2.47 ± 0.60	9.13 ± 0.50	2.66 ± 0.41	11.14 ± 1.03	2.96 ± 0.57
Granuloma or turpentine	8.18 ± 2.40	1.98 ± 0.70	8.43 ± 1.45	1.31 ± 0.22*	2.42 ± 0.43*	0.99 ± 0.13*	3.99 ± 0.22*	1.77 ± 0.18†
Ratio								
L (tumor)/M	34.2 ± 9.8	2.7 ± 0.7	33.0 ± 16.8	5.7 ± 1.9	45.3 ± 6.5	3.6 ± 0.5	37.6 ± 1.5	7.2 ± 1.6
L (granuloma)/M or L (turpentine)/M	30.0 ± 9.3	2.3 ± 0.8	29.7 ± 9.6	3.0 ± 0.6*	11.9 ± 2.4*	1.3 ± 0.2*	13.6 ± 1.9†	4.3 ± 0.8†
L (tumor)/B	13.9 ± 4.4	2.6 ± 0.8	14.9 ± 2.7	3.5 ± 1.0	16.2 ± 1.7	3.8 ± 0.9	14.6 ± 1.7	3.0 ± 0.6
L (granuloma)/B or L (turpentine)/B	12.4 ± 5.1	2.2 ± 0.5	14.3 ± 2.5	1.8 ± 0.3*	4.3 ± 0.9*	1.4 ± 0.2*	5.3 ± 0.9*	1.8 ± 0.1†

*$P < 0.01$, tumor vs. granuloma or tumor vs. turpentine-induced inflammation.
†$P < 0.05$.

was still increased after 30 min after injection. Another limitation of our study was that only 1 tumor model was used to compare accumulation of the PET pharmaceuticals. Other tumor models should be used to confirm our preliminary results.

CONCLUSION

Our experimental studies demonstrated that ^{14}C-methionine uptake in the granuloma was significantly lower than that in the tumor, whereas ^{18}F-FDG and ^{3}H-FLT were not able to differentiate the granuloma from the tumor. These results suggest that ^{14}C-methionine should have the potential to accurately differentiate malignant tumors from benign lesions, particularly granulomatous lesions.

ACKNOWLEDGMENTS

This study was performed through special coordination funds for promoting science and technology, provided by the Ministry of Education, Culture, Sports, Science, and Technology of the Japanese Government. This work was also supported in part by grants-in-aid for scientific research from the Japan Society for the Promotion of Science and the Japanese Ministry of Education, Culture, Sports, Science, and Technology and by a grant from the Rotary Yoneyama Memorial Foundation, Inc. The authors are grateful to the staffs of the Department of Nuclear Medicine, Central Institute of Isotope Science; Institute for Animal Experimentation, Hokkaido University; and Facility of Radiology, Hokkaido University Hospital for supporting this study. We also thank Eriko Suzuki for continuously supporting this study and Makoto Sato, SHI Accelerator Service Ltd., for ^{18}F-FDG synthesis.

REFERENCES

1. Delbeke D, Rose DM, Chapman WC, et al. Optimal interpretation of FDG PET in the diagnosis, staging and management of pancreatic carcinoma. *J Nucl Med.* 1999;40:1784–1791.
2. Dimitrakopoulou-Strauss A, Strauss LG, Heichel T, et al. The role of quantitative ^{18}F-FDG PET studies for the differentiation of malignant and benign bone lesions. *J Nucl Med.* 2002;43:510–518.
3. Brudin LH, Valind S, Rhodes CG, et al. Fluorine-18 deoxyglucose uptake in sarcoidosis measured with positron emission tomography. *Eur J Nucl Med.* 1994; 21:297–305.
4. Lewis PJ, Salama A. Uptake of fluorine-18-fluorodeoxyglucose in sarcoidosis. *J Nucl Med.* 1994;35:1647–1649.
5. Ohtsuka T, Nomori H, Watanabe K, et al. False-positive findings on [^{18}F]FDG-PET caused by non-neoplastic cellular elements after neoadjuvant chemoradiotherapy for non-small cell lung cancer. *Jpn J Clin Oncol.* 2005;35:271–273.
6. Lorenzen J, de Wit M, Buchert R, Igel B, Bohuslavizki KH. Granulation tissue: pitfall in therapy control with F-18-FDG PET after chemotherapy. *Nuklearmedizin.* 1999;38:333–336.
7. Conessa C, Hervé S, Foehrenbach H, Poncet JL. FDG-PET scan in local follow-up of irradiated head and neck squamous cell carcinomas. *Ann Otol Rhinol Laryngol.* 2004;113:628–635.

8. van Waarde A, Cobben DC, Suurmeijer AJ, et al. Selectivity of ^{18}F-FLT and ^{18}F-FDG for differentiating tumor from inflammation in a rodent model. *J Nucl Med.* 2004;45:695–700.
9. van Waarde A. Jager PL, Ishiwata K, Dierckx RA, Elsinga PH. Comparison of sigma-ligands and metabolic PET tracers for differentiating tumor from inflammation. *J Nucl Med.* 2006;47:150–154.
10. Shields AF, Grierson JR, Dohmen BM, et al. Imaging proliferation in vivo with [F-18]FLT and positron emission tomography. *Nat Med.* 1998;4:1334–1336.
11. Sherley JL, Kelly TJ. Regulation of human thymidine kinase during the cell cycle. *J Biol Chem.* 1988;263:8350–8358.
12. Jacobs AH, Dittmar C, Winkeler A, Garlip G, Heiss WD. Molecular imaging of gliomas. *Mol Imaging.* 2002;1:309–335.
13. Tsuyuguchi N, Sunada I, Ohata K, et al. Evaluation of treatment effects in brain abscess with positron emission tomography: comparison of fluorine-18-fluorodeoxyglucose and carbon-11-methionine. *Ann Nucl Med.* 2003;17:47–51.
14. Kubota K, Kubota R, Yamada S, Tada M. Effects of radiotherapy on the cellular uptake of carbon-14 labeled L-methionine in tumor tissue. *Nucl Med Biol.* 1995;22:193–198.
15. Kubota R, Kubota K, Yamada S, et al. Methionine uptake by tumor tissue: a microautoradiographic comparison with FDG. *J Nucl Med.* 1995;36:484–492.
16. Reinhardt MJ, Kubota K, Yamada S, Iwata R, Yaegashi H. Assessment of cancer recurrence in residual tumors after fractionated radiotherapy: a comparison of fluorodeoxyglucose, L-methionine and thymidine. *J Nucl Med.* 1997;38: 280–287.
17. Zhao S, Kuge Y, Kohanawa M, et al. Extensive FDG uptake and its modification with corticosteroid in a granuloma rat model: an experimental study for differentiating granuloma from tumors. *Eur J Med Mol Imaging.* September 1, 2007 [Epub ahead of print].
18. Zhao S, Kuge Y, Tsukamoto E, et al. Effects of insulin and glucose loading on FDG uptake in experimental malignant tumours and inflammatory lesions. *Eur J Nucl Med.* 2001;28:730–735.
19. Takei T, Kuge Y, Zhao S, et al. Enhanced apoptotic reaction correlates with suppressed tumor glucose utilization after cytotoxic chemotherapy: use of ^{99m}Tc-annexin V, ^{18}F-FDG, and histologic evaluation. *J Nucl Med.* 2005;46:794–799.
20. Yamada Y, Uchida Y, Tatsumi K, et al. Fluorine-18-fluorodeoxyglucose and carbon-11-methionine evaluation of lymphadenopathy in sarcoidosis. *J Nucl Med.* 1998;39:1160–1166.
21. Kubota K, Matsuzawa T, Fujiwara T, et al. Differential diagnosis of AH109A tumor and inflammation by radioscintigraphy with L-[methyl-^{11}C]methionine. *Jpn J Cancer Res.* 1989;80:778–782.
22. Osman S, Danpure HJ. The use of 2-[^{18}F]fluoro-2-deoxy-D-glucose as a potential in vitro agent for labeling human granulocytes for clinical studies by positron emission tomography. *Int J Rad Appl Instrum B.* 1992;19:183–190.
23. Borregaard N. Herlin T. Energy metabolism of human neutrophils during phagocytosis. *J Clin Invest.* 1982;70:550–557.
24. Kubota R, Yamada S, Kubota K, Ishiwata K, Tamahashi N, Ido T. Intratumoral distribution of fluorine-18-fluorodeoxyglucose in vivo: high accumulation in macrophages and granulation tissues studied by microautoradiography. *J Nucl Med.* 1992;33:1972–1980.
25. Saga T, Kawashima H, Araki N, et al. Evaluation of primary brain tumors with FLT-PET: usefulness and limitations. *Clin Nucl Med.* 2006;31:774–780.
26. Yap CS, Czernin J, Fishbein MC, et al. Evaluation of thoracic tumor with ^{18}F-fluorothymidine and ^{18}F-fluorodeoxyglucose-positron emission tomography. *Chest.* 2006;129:393–401.
27. Drent M, du Bois RM, Poletti V. Recent advances in the diagnosis and management of nonspecific interstitial pneumonia. *Curr Opin Pulm Med.* 2003;9:411–417.
28. Inoue T, Kim EE, Wong FC, et al. Comparison of fluorine-18-fluorodeoxyglucose and carbon-11-methionine PET in detection of malignant tumors. *J Nucl Med.* 1996;37:1472–1476.
29. Kubota K, Ishiwata K, Kubota R, et al. Feasibility of fluorine-18-fluorophenylalanine for tumor imaging compared with carbon-11-L-methionine. *J Nucl Med.* 1996; 37:320–325.

Eur J Nucl Med Mol Imaging (2007) 34:2096–2105
DOI 10.1007/s00259-007-0529-8

ORIGINAL ARTICLE

Extensive FDG uptake and its modification with corticosteroid in a granuloma rat model: an experimental study for differentiating granuloma from tumors

Songji Zhao · Yuji Kuge · Masashi Kohanawa · Toshiyuki Takahashi · Hidekazu Kawashima · Takashi Temma · Toshiki Takei · Yan Zhao · Koh-ichi Seki · Nagara Tamaki

Received: 6 July 2006 / Accepted: 3 July 2007 / Published online: 1 September 2007

Abstract
Introduction Increased ^{18}F-fluorodeoxyglucose (FDG) uptake in inflammatory lesions, particularly in granulomatous inflammation (e.g., sarcoidosis), makes it difficult to differentiate malignant tumors from benign lesions and is the main source of false-positive FDG-PET findings in oncology. Here, we developed a rat granuloma model and examined FDG uptake in the granuloma. The effects of corticosteroid on FDG uptake in the granuloma were compared with those in a malignant tumor.

Methods Rats were inoculated with *Mycobacterium bovis* bacillus Calmette-Guérin (BCG) or allogenic hepatoma cells, and subdivided into control and pretreated (methylprednisolone acetate, 8 mg/kg i.m.) groups. Radioactivity in tissues was determined 1 h after the FDG injection. FDG-PET was performed in rats bearing BCG granulomas or tumors before and after prednisolone treatment.

Results Mature epithelioid cell granuloma-formation and massive lymphocyte-infiltration were observed in the control group of granuloma, histologically similar to sarcoidosis. The mean FDG uptake in the granuloma was comparable to that in the hepatoma. Prednisolone reduced epithelioid cell granuloma-formation and lymphocyte-infiltration. Prednisolone significantly decreased the level of FDG uptake in the granuloma (52% of control), but not in the hepatoma. The FDG uptake levels in the granulomas and tumors were clearly imaged with PET.

Conclusion We developed an intramuscular granuloma rat model that showed a high FDG uptake comparable to that of the tumor. The effect of prednisolone pretreatment on FDG uptake was greater in the granuloma than in the tumor. These results suggest that BCG-induced granuloma may be a valuable model and may provide a biological basis for FDG studies.

Keywords FDG · Granuloma · Tumor · Corticosteroid · Rat

S. Zhao · T. Takei · Y. Zhao · N. Tamaki (✉)
Department of Nuclear Medicine, Graduate School of Medicine, Hokkaido University,
Kita 15 Nishi 7, Kita-ku,
Sapporo 060-8638, Japan
e-mail: natamaki@med.hokudai.ac.jp

Y. Kuge
Department of Molecular Imaging, Graduate School of Medicine, Hokkaido University,
Sapporo, Japan

Y. Kuge · H. Kawashima · T. Temma
Department of Patho-functional Bioanalysis, Graduate School of Pharmaceutical Sciences, Kyoto University,
Kyoto, Japan

M. Kohanawa
Department of Microbiology, Graduate School of Medicine, Hokkaido University,
Sapporo, Japan

T. Takahashi
Department of Pathology, Hokkaido Gastroenterology Hospital,
Sapporo, Japan

K. Seki
Central Institute of Isotope Science, Hokkaido University,
Sapporo, Japan

Introduction

PET using FDG has become a very useful imaging tool not only for detecting and staging malignant tumors but also for monitoring therapy response and for differentiating malignant tumors from benign lesions [1]. These applications are

based on the increased FDG uptake due to enhanced glucose utilization in most tumors. Recent investigations, however, have shown that FDG accumulates not only in malignant tumors but also in various forms of inflammatory lesions, particularly in granulomatous lesions, such as sarcoidosis or active inflammatory processes after chemoradiotherapy [2–4]. Increased FDG uptake in such inflammatory lesions makes it difficult to differentiate malignant tumors from benign lesions and is the main source of false-positive FDG-PET findings in oncology [5]. Thus, it is of great importance to investigate FDG uptake in granulomatous lesions for accurately differentiating malignant and benign lesions by FDG-PET. However, FDG uptake in granulomatous lesions remains unclarified, mainly due to the lack of suitable animal models. To the best of our knowledge, there have been no studies of FDG uptake in experimental granulomatous lesions to date, although increased FDG uptake in inflammatory lesions has been reported in experimental inflammation induced by intramuscular injection of *Staphylococcus aureus* (*S. aureus*) or turpentine oil [5, 6]. Thus, we developed a granuloma rat model.

In the present study, we induced granuloma in the muscle of rats by BCG inoculation and examined FDG uptake in the granuloma in comparison with that in a tumor. In addition, we determined the effect of predonisolone pretreatment on FDG uptake in the granuloma to evaluate whether corticosteroid pretreatment facilitates the differentiation of malignant tumors from benign lesions by FDG -PET.

Materials and methods

Animal studies

All experimental protocols were approved by the Laboratory Animal Care and Use Committee of Hokkaido University. Eight-week-old male Wistar King Aptekman/hok (WKAH) rats (supplied by the Experimental Animal Institute, Graduate School of Medicine, Hokkaido University, Sapporo) were used in all experiments. The *Mycobacterium bovis* bacillus Calmette-Guérin (BCG), Japan strain, was grown on Middlebrook 7H11 agar (Difco Laboratories, Detroit, Mich), suspended in PBS with 0.05% Tween 20, and stocked at −80°C. A 1×10^7 CFU/rat dose of BCG, which was determined in our preliminary experiments, was inoculated into the left calf muscle of rats to induce appropriate sizes and numbers of granulomatous lesions. To produce an experimental tumor, rats were inoculated with a suspension of allogenic hepatoma cells (KDH-8, 1×10^6 cells/rat) into the left calf muscle [7]. Nineteen days after BCG inoculation or 14 days after KDH-8 inoculation, when the BCG-induced granulomatous lesions were 3–8 mm in diameter, or when the KDH-8-induced tumor tissues were 20–30 mm in diameter, the rats were fasted overnight and then randomly divided into two subgroups: prednisolone (PRE)-pretreated and control (untreated) (n=5–6, in each group). The sizes of the granuloma and tumors were checked under palpation, and then measured using calipers. The rats in the PRE-pretreated group were intramuscularly injected with methylprednisolone acetate (8 mg/kg body weight) in the left brachialis muscle 20 h before the FDG injection, according to the methods reported by Gemma et al. [8]. Each rat was anaesthetized with pentobarbital (50 mg/kg body weight, i.p.) and was injected in the tail vein with 5–6 MBq of FDG. The rats were kept under anaesthesia for the rest of the experiment. Sixty minutes after the FDG injection, the animals were sacrificed and tumor, granuloma tissues, and other organs were excised. The tissues and blood samples were weighed, and radioactivity was determined using a gamma counter (1480 WIZARDTM3″; Wallac Co., Ltd.). FDG uptake in the tissues was expressed as the percentage of injected dose per gram of tissue after being normalized to the animal's weight (%ID/g × kg). The lesion (granuloma or tumor)-to-muscle (L/M) ratio and the lesion (granuloma or tumor)-to-blood (L/B) ratio of FDG uptake were calculated from the (%ID/g)×kg value of each tissue [6]. By using tissue samples from the tumors and granulomas, frozen specimens and formalin-fixed, paraffin-embedded specimens were prepared for subsequent histologic staining. Blood samples for glucose measurement were obtained immediately before FDG injection and immediately before sacrifice. Blood glucose level was determined using a biochemical analyzer (MediSense, Dainobot Co., Ltd.).

Histochemical studies

Immunohistochemical staining for immune-associated antigen (Ia) was performed using a monoclonal antibody (mAb) (mouse IgG, MRC OX-6, Oxford Biotechnology Ltd.) that recognizes a monomorphic determinant of the rat Ia, MHC class II present on B lymphocytes, dendritic cells, some macrophages, and certain ephithelial cells. To further support the Ia-positive (Ia+) staining, other mAbs, namely, MRC OX-3 and MRC OX-17 were also used. The MRC OX-3 mAb (Serotec), a mouse anti-rat RT1Bu mAb, recognizes a polymorphic determinant of the rat Ia-A antigen RT1Bu (class II polymorphic) found on B cells, dendritic cells, and certain epithelial cells. The MRC OX-17 mAb (Serotec) recognizes a monomorphic determinant of the rat RT-1D (class II monomorphic), the rat homologue of the mouse Ia-E, which has a similar structure to the Ia-A antigen and reacts with anti-Ia alloantibodies. The MRC OX-17 mAb does not cross-react with the rat Ia-A (RT-1B) antigen, while both class II monomorphic MRC OX-6 and MRC OX-17 mAbs were active against determinants found in all rat strains. The different cell types were characterized

by positive staining with several monoclonal antibodies, i.e., RM-4 (Cosmo Bio Co., Ltd.) for macrophages, MRC OX-8 (mouse anti-rat CD8 alpha mAb, Serotec) for nonhelper T cells, and MRC OX-35 (mouse anti-rat CD4 mAb, Serotec) for helper T cells. The epithelioid cells and macrophages found around epithelioid cell granulomas were determined by positive staining with RM-4 (Fig. 2c). T cell subsets were characterized using MRC OX-35 and MRC OX-8.

The formalin-fixed, paraffin-embedded tumor and granuloma tissues were sectioned at 3 μm thickness and stained with hematoxylin and eosin (HE), whereas the frozen granuloma tissues were cut at 4 μm thickness. Immunohistochemical staining was carried out according to a standard immunostaining procedure [7–9]. Briefly, after deparaffization and rehydration (for MRC OX-6, MRC OX-8, and RM-4 mAbs), tissue sections were heated at 121°C for 15 min in 10 mM sodium citrate buffer, pH 6.0, for antigen retrieval (MRC OX-6 mAb). Frozen sections were fixed in ethanol (for MRC OX-3, MRC OX-17, and MRC OX-35 mAbs). Endogenous peroxidase activity was blocked for 5 min in methanol containing 3% hydrogen peroxide. Thereafter, slides were incubated with primary antibodies for 30 min at room temperature. The bound antibody was visualized by the avidin/biotin conjugate immunoperoxidase procedure using the HISTOFINE SAB 2 system HRP (Dako, Japan) and 3,3′-diaminobenzidine tetrahydrochloride (DAB) (Dako, Japan). Counterstaining was performed with hematoxylin.

PET imaging

PET experiments were performed in rats bearing BCG granulomas or KDH-8 tumors before (control) and after a prednisolone treatment. Eighteen days after BCG inoculation or 13 days after KDH-8 inoculation, the rats (n=3 for BCG granulomas and KDH-8 tumors, respectively) were fasted overnight, and anesthetized with pentobarbital (50 mg/kg body weight, i.p.). The rats were placed in a PET scanner (SHR-7700L, Hamamatsu Photonics, Hamamatsu, Japan) in a supine position and injected with FDG (28–30 MBq/rat) in the lateral tail vein. Sixty minutes after the injection of FDG, the rats underwent a first PET scanning for 15 min. After the PET scanning, the rats were treated with methylprednisolone acetate (8 mg/kg body weight). Twenty hours after the prednisolone treatment, a second FDG-PET scan was carried out using the same procedures as the first PET scan. The PET images were reconstructed by a standard filtered back-projection using a Hamming filter into a 256 × 256 × 31 (0.6 × 0.6 × 3.6 mm) matrix. The spatial resolution of the reconstructed images was 2.7 mm in the plane [10].

Statistical analysis

All values are expressed as mean ± standard deviation. To evaluate the significance of the differences in the values obtained between the control group and the treated group, an unpaired student's t test was performed.

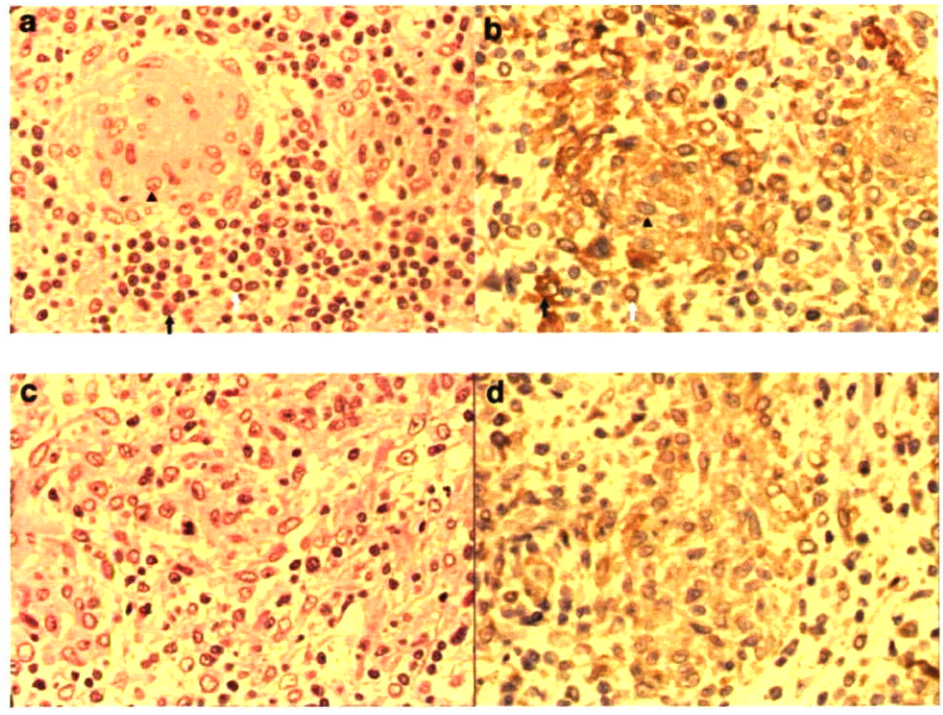

Fig. 1 Microscopic images (x 400) of HE-stained (**a**, **c**) and immunostained granuloma (**b**, **d**) for Ia antigen with MRC OX-6 mAb in control (**a**, **b**) and pretreated rats (**c**, **d**). **a** Mature epithelioid cell granuloma-formation and massive lymphocyte-infiltration. **b** Infiltrations of Ia-positive epithelioid cells and macrophages in granuloma and Ia-positive lymphocytes in granuloma periphery (for MRC OX-6). **c** Reduction of epithelioid cell granuloma-formation and lymphocyte-infiltration. **d** Reduction of infiltrations of Ia+ macrophages and Ia+ lymphocytes around granuloma. *Black arrow head* indicates epithelioid cell granuloma; *black arrow*, macrophage infiltration; *white arrow*, lymphocyte infiltration

A two-tailed value of $P<0.05$ was considered significant. The statistical program Stat View 5.0 was used for the data assessment.

Results

Histopathological findings

In the control animals inoculated with BCG, mature epithelioid cell granuloma-formation and massive lymphocyte-infiltration were observed in the calf muscle (Fig. 1a). Immunohistochemical staining with the MRC OX-6 mAb showed the accumulation of Ia^+ macrophages and Ia^+ lymphocytes into the periphery of the granuloma (Fig. 1b). In the prednisolone pretreatment group, reduction in the levels of epithelioid cell granuloma-formation and lymphocyte-infiltration and in the levels of Ia^+ macrophage-infiltration and Ia^+ lymphocyte-infiltration were observed (Fig. 1c and d). Immunostaining with MRC OX-3 and MRC OX-17 mAbs also showed the accumulation of Ia+ macrophages and Ia+ lymphocytes into the periphery of the granulomas in the control animals (Fig. 2a and b).

The different cell types in the granulomatous tissues were characterized by positive staining with several monoclonal antibodies. The epithelioid cells and macrophages determined by positive staining with RM-4 were found in the epithelioid cell granulomas and around epithelioid cell granulomas (Fig. 2c). Immunohistochemical staining of CD4 and CD8 showed numerous CD4+ (helper T cells) and CD8+ T cells (nonhelper T cells) surrounding the granulomas (Fig. 2d and e).

In the control animals inoculated with KDH-8, massive viable and proliferating cancer cells were observed by HE staining (Fig. 3a). Immunohistochemical staining with the MRC OX-6 mAb showed scattered Ia^+ macrophages-infiltration and Ia^+ lymphocytes-infiltration into the viable tumor cells (Fig. 3b). There were no histopathological changes for tumor tissue after treatment with prednisolone (Fig. 3c and d).

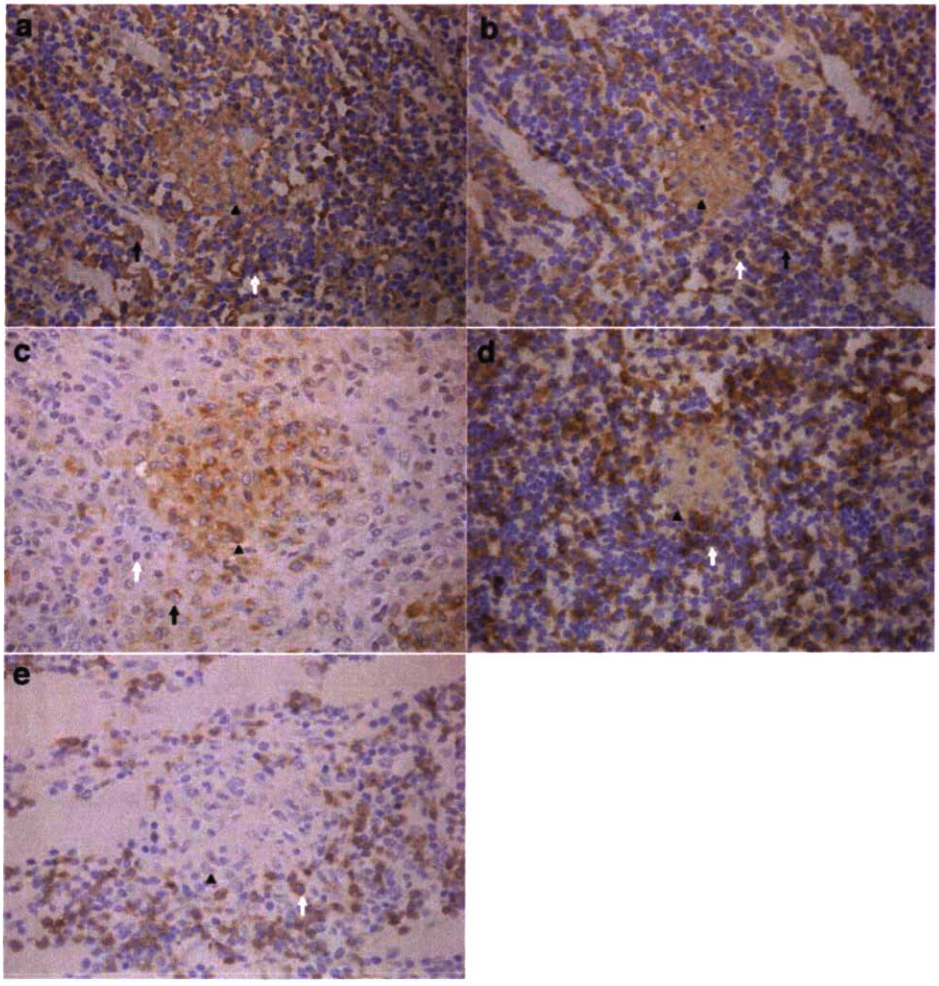

Fig. 2 Microscopic images (x 400) of immunostained for Ia antigen with MRC OX-3 (**a**), MRC OX-17 mAbs (**b**), and cell type characterization (**c**-**e**) in granulomas of control rats. **a** Accumulation of Ia+ epithelioid cells, Ia+ macrophages and Ia+ lymphocytes were characterized by MRC OX-3 mAb. **b** Accumulation of Ia+ epithelioid cells, Ia+ macrophages, and Ia+ lymphocytes were characterized by MRC OX-17 mAb. **c** The epithelioid cells and macrophages were determined by RM-4 positive staining. **d** CD4+ T cells (helper T cells) were determined by MRC OX-35 mAb. **e** CD8+ T cells (nonhelper T cells) were determined by MRC OX-8 mAb. *Black arrow head* indicates epithelioid cell granuloma; *black arrow*, macrophage infiltration; *white arrow*, lymphocyte infiltration